

Exhibit A

Dr. Koshimizu's Curriculum Vitae

Exhibit A

Curriculum Vitae

June 12, 2007

Name: Uichi KOSHIMIZU

Degree: Ph.D. (Medicine)

Present Address: (Laboratory)

Asubio Pharma Co., Ltd.

Biomedical Research Laboratories

1-1-1 Wakayama-dai, Shimamoto-cho, Mishima-gun,

Osaka 618-8513, Japan

Tel: +81-75-962-8304

Fax: +81-75-962-6448

E-mail: koshimizu.uichi.ss@asubio.co.jp

(Home)

15-1 Hyakuyama, Shimamoto-cho, Mishima-gun,

Osaka 618-0021, Japan

Position: Manager and chief researcher of Medical Biotechnology Group

Date of Birth: June 21, 1965 (Age:41)

Nationality: Japanese

Education and Positions:

1984-1988 Faculty of Agriculture at Meiji University (Knagawa, Japan)
Advisor: Prof. H. Nagasawa

1988-1994 Ph.D. candidate of Osaka University Medical School (Osaka, Japan)
Advisor: Prof. Y. Nishimune
(Research Insitute for Microbial Diseases)

1993-1995 Research fellow, National Institute of Genetics (Mishima, Japan)
Advisor: Prof. N. Nakatsuji

Received Ph.D. in March, 1994, from Osaka University Medical School

1995-2001 Assistant Professor & Lecturer, Osaka University Medical School (Osaka, Japan)

**2001-2007 Senior Researcher,
Suntory Biomedical Research Co. Ltd.
(renamed as Asubio Pharma Co. Ltd)**

2007- Manager and chief researcher of Medical Biotechnology Group

**Awards: Fellowships of the Japan Society for the Promotion of Science
for Junior Scientists (1992-1994, 1994- 1995)**

**Memberships: Japanese Society of Developmental Biologists
Molecular Biological Society of Japan
Japanese Society of Regenerative Medicine
Japan Society of Gene Therapy
International Society for Stem Cell Research**

Publication List

Articles (in English): 45

Reviews (in English): 1

Reviews (in Japanese): 25

Patent specifications: 4

The important articles

1. U. Koshimizu, D. Watanabe, Y. Tajima, and Y. Nishimune
Effects of *W* (*c-kit*) Gene Mutation on Gametogenesis in Male Mice: Agametic Tubular Segments in W^f/W^f Mice. *Development* 114:861-867 (1992)
2. T. Tono, T. Tsujimura, U. Koshimizu, T. Kasugai, S. Adachi, K. Isozaki, S.-I. Nishikawa, M. Morimoto, Y. Nishimune, and Y. Kitamura
c-kit Gene Was Not Transcribed in Cultured Mast Cells of Mast Cell- Deficient W^{sh}/W^{sh} Mice That Have a Normal Number of Erythrocytes and a Normal *c-kit* Coding Region. *Blood* 80:1448-1453 (1992)
3. U. Koshimizu, D. Watanabe, Y. Tajima, and Y. Nishimune
A Novel Stage-Specific Differentiation Antigen Is Expressed on Mouse Testicular Germ Cells during Early Meiotic Prophase. *Biol. Reprod.* 49:875-884 (1993)
4. T. Tsujimura, U. Koshimizu, H. Katoh, K. Isozaki, Y. Kanakura, T. Tono, S. Adachi, T. Kasugai, H. Tei, Y. Nishimune, S. Nomura, and Y. Kitamura
Mast Cell Number in the Skin of Heterozygotes Reflects the Molecular Nature of *c-kit* Mutation. *Blood* 81:2530-2538 (1993)
5. U. Koshimizu, T. Tsujimura, K. Isozaki, S. Nomura, T. Furitsu, Y. Kanakura, Y. Kitamura and Y. Nishimune
 W^r Mutation of *c-kit* Receptor Affects Its Post-Translational Processing and Extracellular Expression. *Oncogene* 9:157-162 (1994)
6. D. Watanabe, K. Yamada, Y. Nishina, Y. Tajima, U. Koshimizu, A. Nagata, and Y. Nishimune
Molecular Cloning of a Novel Ca^{2+} -binding Protein (Calmegin) Specifically Expressed during Male Meiotic Germ Cell Development. *J. Biol. Chem.* 269:7744-7749 (1994)
7. K. Isozaki, T. Tsujimura, S. Nomura, E. Morii, U. Koshimizu, Y. Nishimune, and Y. Kitamura
Cell Type-Specific Deficiency of *c-kit* Gene Expression in Mutant Mice of *mi/mi* Genotype. *Am. J. Pathol.* 145:827-836 (1994)

8. U. Koshimizu, H. Nishioka, D. Watanabe, K. Dohmae and Y. Nishimune
Characterization of A Novel Spermatogenic Cell Antigen Specific for Early Stages of Germ Cells in Mouse Testis.
Mol. Reprod. Dev. 40:221-227 (1995)
9. U. Koshimizu, M. Watanabe and N. Nakatsuji
Retinoic Acid Is a Potent Growth Activator of Mouse Primordial Germ Cells *in vitro*.
Dev. Biol. 168: 683-685 (1995)
10. U. Koshimizu, T. Taga, M. Watanabe, M. Saito, Y. Shirayoshi, T. Kishimoto and N. Nakatsuji
Functional Requirement of gp130-mediated Signaling for Growth and Survival of Mouse Primordial Germ Cells *in vitro* and Derivation of Embryonic Germ (EG) Cells.
Development 122:1235-1242 (1996)
11. U. Koshimizu, H. Takahashi, Y. Yoshida and T. Nakamura
cDNA Cloning, Genomic Organization, and Chromosomal Localization of Mouse LIM Motif- Containing Kinase *Limk-2*.
Biochem. Biophys. Res. Commun. 241:243-250 (1997)
12. U. Koshimizu, K. Matsumoto, T. Nakamura
Hepatotrophic Activities of HGF in Liver Regeneration After Injury and the Clinical Potentiality for Liver Diseases. *in* "Liver and Environmental Xenobiotics" (S.V.S. Rana and K. Taketa, *eds.*), Narosa-Verlag, pp.220-229 (1997)
13. H. Ohmichi, U. Koshimizu, K. Matsumoto, T. Nakamura
Hepatocyte Growth Factor (HGF) Acts as a Mesenchyme-Derived Morphogenic Factor during Fetal Lung Development. *Development* 125:1315-1324 (1998)
14. H. Takahashi, U. Koshimizu, and T. Nakamura
A Novel Transcript Encoding Truncated LIM-Kinase 2 Is Specifically Expressed in Male Germ Cells Undergoing Meiosis.
Biochem. Biophys. Res. Commun. 249:128-145 (1998)
15. K. Kitajima, U. Koshimizu, and T. Nakamura
Expression of a Novel Type of Classic Cadherin, PB-Cadherin in Developing Brain and Limb Buds.
Dev. Dyn. 215:206-214 (1999)
16. O. Amano, U. Koshimizu, T. Nakamura, and S.Iseki
Hepatocyte Growth Factor (HGF) Enhances Bone and Cartilage Formation during Embryonic Mouse Mandibular Development *in vitro*.
Arch. Oral Biol. 44:935-46 (1999)
17. T. Kunisada, H. Yamazaki, T. Hirobe, S. Kamei, M. Omoteno, H. Tagaya, U. Koshimizu, T. Nakamura, and S. Hayashi
Keratinocyte Expression of Transgenic Hepatocyte Growth Factor (HGF) Affects Melanocyte Development, Leading to Dermal Melanocytosis.
Mech. Dev. 94:67-78 (2000)
18. Takahashi, U. Koshimizu, H. Abe, T. Obinata, and T. Nakamura

Functional Involvement of *Xenopus* LIM-Kinases in Progression of Oocyte Maturation.
Dev. Biol. 229:554-67 (2001)

19. O. Amano, A. Yamane, M. Shimada, U. Koshimizu, T. Nakamura, and S. Iseki.
Hepatocyte Growth Factor Is Essential for Migration of Myogenic Cells and Promotes Their Proliferation during the Early Periods of Tongue Morphogenesis in Mouse Embryos.
Dev. Dyn. 223:169-79 (2002)
20. H. Takahashi, U. Koshimizu, J. Miyazaki, and T. Nakamura
Impaired Spermatogenic Ability of Testicular Germ Cells in Mice Deficient in the LIM-Kinase 2 Gene.
Dev. Biol. 241:259-72 (2002)
21. K. Kitajima, U. Koshimizu, H. Takahashi, M. Tahara, K. Matsumoto, K. Miyamoto, and T. Nakamura
Molecular Cloning of AMSH-Like Molecule and Its Unique Expression in Testis.
Biochem. Biophys. Acta (2003)
22. S. Yuasa, Y. Itabashi, U. Koshimizu, T. Tanaka, K. Sugimura, M. Kinoshita, F. Hattori, S. Fukami, T. Shimazaki, S. Ogawa, H. Okano, and K. Fukuda.
Transient inhibition of BMP signaling by Noggin induces cardiomyocyte differentiation of mouse embryonic stem cells.
Nat. Biotechnol. 23:607-11(2005)
23. M. Nagaoka, U. Koshimizu, S. Yuasa, F. Hattori, H. Chen, T. Tanaka, M. Okabe, K. Fukuda, and T. Akaike
E-cadherin-coated plates induce rapid proliferation, efficient transfection, and low LIF dependency of pluripotent ES cells without colony formation..
PLoS ONE. 1: e15 (2006)
24. M. Nagaoka, H. Ise, I. Harada, U. Koshimizu, A. Maruyama, and T. Akaike
Embryonic undifferentiated cells show the scattering activity on E-cadherin-immobilized surface. *J. Cell. Biochem.* (in press)
25. M. Tamamori-Adachi, H. Takagi, K. Hashimoto, K. Goto, T. Hidaka, U. Koshimizu, K. Yamada, I. Goto, J. Kawauchi, K. I. Nakayama, N. Inomata, and S. Kitajima
in situ proliferation of cardiomyocytes by nuclear cyclin D1/CDK4 and Skp2 improves heart failure.(submitted)
26. T. Tanaka, M. Kadokura, K. Kawashima, S. Oikawa, K. Fukuda, and U. Koshimizu
Transient activation of canonical Wnt signaling induces cardiomyocyte differentiation of embryonic stem cells. (in preparation)

Patent specifications

1. "Method of inducing the differentiation of stem cells into myocardial cells"
(WO2005-033298)
2. "Method of growing myocardial cells" (WO2005-049822)
3. "Method of proliferating pluripotent cells" (WO2005-090557)
4. "Method of preparation of cardiomyocytes from pluripotent stem cells"
(PCT/JP2007/59242)

Exhibit B

References Cited in Dr. Koshimizu's Declaration

S. van den Heuvel and E. Harlow

**“Distinct Roles for Cyclin-Dependent Kinases in
Cell Cycle Control”**

calcium phosphate coprecipitation technique. After 48 hours, transfected cells were washed with medium containing 2 mM EDTA and then with culture medium. Cells were then challenged with HIV-1 LAI (corresponding to 0.5 μ g of p25, which is equivalent to about 40 particles per cell) for 6 hours in the absence or presence of inhibitors. Cells were first washed in medium containing 2 mM EDTA and then washed once with trypsin before incubation (5 min at 37°C) in 5 ml of trypsin. Cells were then replated in 75-cm² flasks containing fresh culture medium and incubated at 37°C for 24 hours. One-milliliter portions of each supernatant were then used to infect CEM cells (5 \times 10⁶). The production of HIV-1 (as determined by ELISA of p25) in CEM cultures was measured by assaying culture supernatants 7, 9, and 11 days later. The expression of CD4 antigen on the cell surface of transfected cells was carried out 48 hours after trypsin treatment by FACS analysis with mAb OKT4. [P. R. Rao, M. A. Talle, P. C. Kung, G. Goldstein, *Cell Immunol.* 80, 310 (1983)]. The expression of human CD26 was determined

after immunoprecipitation (see Fig. 4, legend).
33. Supported by grants from Institut Pasteur, Paris, and Agence Nationale de la Recherche sur le SIDA. C.C. and E.J. were supported by Association des Artistes contre le SIDA. We thank I. Marié and N. Robert for assistance; A. Laurent-Crawford, M. A. Rey-Cuillé, and D. Cointe for discussion during this work; and B. Bauvois for advice on the assay of DPP IV activity and critical reading of the manuscript. Monoclonal antibody IF7 was kindly provided by C. Morimoto, Dana-Farber Cancer Institute, Harvard Medical School, Boston. The pLXSN-CD4 plasmid was obtained from O. Schwartz, Institut Pasteur, Paris. Plasmid pKG5 expressing human CD26 was kindly provided by B. Fleischer, Universität Mainz. Additional thanks go to R. Siraganian and B. R. G. Williams for critical reading of the manuscript. Special acknowledgments are forwarded to L. Montagnier for advice and continual support during the realization of this work.

1 October 1993; accepted 18 November 1993

Distinct Roles for Cyclin-Dependent Kinases in Cell Cycle Control

Sander van den Heuvel* and Ed Harlow

The key cell-cycle regulator Cdc2 belongs to a family of cyclin-dependent kinases in higher eukaryotes. Dominant-negative mutations were used to address the requirement for kinases of this family in progression through the human cell cycle. A dominant-negative Cdc2 mutant arrested cells at the G₂ to M phase transition, whereas mutants of the cyclin-dependent kinases Cdk2 and Cdk3 caused a G₁ block. The mutant phenotypes were specifically rescued by the corresponding wild-type kinases. These data reveal that Cdk3, in addition to Cdc2 and Cdk2, executes a distinct and essential function in the mammalian cell cycle.

Cell division is controlled by way of a complex network of biochemical signals that are similar in all eukaryotic cells. Together, these signals regulate specific transitions in the cell cycle. The best characterized transitions are those from G₁ to S phase and from G₂ to mitosis. In yeast, passage through both transition points is regulated by the same protein kinase, the product of the *CDC28* or *cdc2⁺* gene for *Saccharomyces cerevisiae* and *Schizosaccharomyces pombe*, respectively (1). The Cdc2-CDC28 catalytic subunit requires association with a cyclin regulatory subunit for kinase activity (2), and different cyclins are involved in the G₁/S transition (G₁ cyclins) and the G₂/M transition (mitotic cyclins). Multicellular eukaryotes appear to have developed a higher degree of regulation. They express multiple cyclins, like yeast, but also contain multiple catalytic subunits that can interact with these cyclins. Whereas p34^{cdc2} is active and essential at the G₂/M transition (3, 4), a closely related kinase, p33^{cdk2}, has been implicated in

the initiation of DNA replication (3, 5, 6).

Twelve human protein kinases have been described that share extensive amino acid sequence identity with p34^{cdc2} (7–10). These kinases are named temporarily after their amino acid sequence in the PSTAIRE-region (11), a domain that is conserved between yeast and human Cdc2. Alternatively, they are designated as cyclin-dependent kinases either when a cyclin partner is identified or when they complement yeast *cdc2-cdc28* mutations. In mammalian cells, Cdc2 associates mainly with A- and B-type cyclins; Cdk2 associates with cyclins A, E, and D; and Cdk4 (formerly PSK-J3), Cdk5 (previously PSSALRE), and Cdk6 (previously PLSTIRE) associate with D-type cyclins (5, 8, 10, 12, 13). Although Cdk3 has never been found in association with cyclins, because of high sequence identity with both Cdc2 and Cdk2 and the ability to complement *cdc28* mutations in yeast, it is classified as a cyclin-dependent kinase (7).

The existence of a family of Cdc2-related genes suggests that other kinases, in addition to Cdc2 and Cdk2, may regulate distinct steps in the cell cycle. To investigate the requirement for the other kinases

in cell cycle progression, we examined the phenotypic consequences of the inactivation of each kinase. We generated dominant-negative mutations for each Cdc2-related kinase and expressed these mutant forms in human cells. When expressed at high levels, dominant-negative mutations inactivate the function of the wild-type protein by competing for essential interacting molecules (14). Data from previous structure-function studies predicted that the mutation of Asp¹⁴⁵ in Cdk2 (Asp¹⁴⁶ in Cdc2) might generate dominant-negative mutants. This residue is conserved in all protein kinases and is part of an amino acid stretch, KLAD*FGLAR (11) (* marks point of mutation), that is identical in all Cdc2-related genes (7, 15). The equivalent Asp residue in 3',5'-adenosine monophosphate (cAMP)-dependent kinase is known to be essential in the phospho-transfer reaction (16). On the basis of the crystal structure data, this residue presumably chelates Mg²⁺ and orients the β - and γ -phosphates of magnesium adenosine triphosphate (Mg²⁺ATP) in the catalytic cleft of the enzyme (17). Moreover, an Asp to Asn point mutation at this position has been identified in one of the two dominant-negative mutant alleles that have been found for CDC28 in yeast (18). Finally, this residue is located outside the regions of *cdc2* that are implicated in binding cyclin and p13^{suc1} subunits (19).

To determine whether dominant-negative inhibition could lead to specific loss of function, we tested the effects of the Asp to Asn mutation in Cdc2 and Cdk2. For each kinase, four versions were generated: wild type (wt) and mutant, each untagged or modified with an influenza hemagglutinin (HA) epitope tag at the COOH-terminus to allow discrimination between endogenous and exogenous kinases (20). When expressed from the inducible GAL4 promoter in yeast, wild-type tagged and untagged forms of Cdc2 and Cdk2 were able to rescue the *cdc28-4* allele at the nonpermissive temperature (36°C), indicating that the tagged kinases were functional (21). The corresponding mutant forms could not rescue *cdc28* mutations at the nonpermissive temperature. Moreover, these mutants interfered with proliferation when induced at the permissive temperature (21).

The wild-type and mutant kinases were cloned under the control of the cytomegalovirus (CMV) promoter and were transiently transfected into human U2OS osteosarcoma cells (20, 22). The expression levels of the wild-type and mutant proteins were similar (Fig. 1, B and C). However, in vitro histone H1 kinase activity was only associated with the wild-type kinases (Fig. 1D). The epitope-tagged forms of both wild-type and mutant Cdc2 appeared to associate with

cyclins. The epitope-tagged mutant kinases functionally inhibited wild-type kinases.

If wild-type kinases are essential for cell cycle progression, then dominant-negative mutants should arrest cells at specific transition points. To test this, we transfected human U2OS cells with wild-type or mutant kinases and analyzed the cells for growth and morphology. Transfection of wild-type Cdc2 or Cdk2 resulted in no apparent effect on cell growth or morphology. Transfection of wild-type Cdk3 resulted in a slight growth defect.

Expression of dominant-negative Cdc2 mutants resulted in a growth defect. The Cdc2 mutants arrested cells at the G₂/M transition. This was evident from the fact that the cells were arrested at the G₂/M transition of the cell cycle. The cells were arrested at the G₂/M transition of the cell cycle. The cells were arrested at the G₂/M transition of the cell cycle.

To determine whether the growth defect was due to the expression of the mutant kinases, we transfected cells with wild-type or mutant kinases and analyzed the cells for growth and morphology. Transfection of wild-type Cdc2 or Cdk2 resulted in no apparent effect on cell growth or morphology. Transfection of wild-type Cdk3 resulted in a slight growth defect.

If wild-type kinases are essential for cell cycle progression, then dominant-negative mutants should arrest cells at specific transition points. To test this, we transfected human U2OS cells with wild-type or mutant kinases and analyzed the cells for growth and morphology. Transfection of wild-type Cdc2 or Cdk2 resulted in no apparent effect on cell growth or morphology. Transfection of wild-type Cdk3 resulted in a slight growth defect.

Massachusetts General Hospital Cancer Center, Charlestown, MA 02129.

*To whom correspondence should be addressed.

mined the inactivated Cdc2- Δ mutant expressed at mutations wild-type interact-
previous-
cted that Asp¹⁴⁶ in
t-negative
y in all
mino acid
(* marks
ical in all
equivalent
onophos-
is known
transfer re-
the crystal
ably ched
y-phos-
triphos-
ic cleft of
sp to Asn
has been
dominant-
ave been
Finally,
regions of
ng cyclin

cyclins A and B1, like endogenous Cdk2. The equivalent forms of Cdk2 bound to cyclins E and A (23). Thus, the Asp to Asn mutation in Cdc2 and Cdk2 abolished their function as kinases but did not affect their ability to associate with cyclins. If wild-type Cdk2 and Cdc2 are required at specific times in the cell cycle, overexpression of dominant-negative mutants should block cell cycle progression when their kinase activity is required. We evaluated such phenotypes in transient transfection assays by including an expression plasmid for the B cell surface marker CD20. Transfected cells were identified by CD20 staining, and the cell cycle profile of the CD20-positive cells was determined by flow cytometry (22). Within the same experiment, the G₁, S, and G₂/M populations varied by a few percent at most between samples that were independently transfected with the same plasmids. Four different human cell lines with high transfection efficiencies were used in these experiments: U2OS and Saos-2 osteosarcoma cells, C33A cervical carcinoma cells, and T98G glioblastoma cells.

Expression of mutant Cdk2 and mutant Cdc2 changed the cell cycle distribution. The Cdk2 mutant (Cdk2-dn) caused a large increase in the G₁ population, whereas the Cdc2 mutant (Cdc2-dn) led to an increased G₂/M population (Fig. 1A). Transfection of wild-type Cdc2 or Cdk2 did not affect the cell cycle distribution (24). However, the effect of the mutant kinase could be overcome in each case by the cotransfection of a plasmid expressing the corresponding wild-type kinase (Fig. 1A). Whereas the Cdk2-dn caused an effect in all cell lines tested, a Cdc2-dn effect was not observed in C33A cells (25).

Together, these data suggest that the arrests observed after the overexpression of mutant Cdk2 or Cdc2 are the result of specific inhibition of the activity of the endogenous wild-type kinases. The timing of the arrest is distinct for the Cdc2 and Cdk2 mutants and is consistent with the timing of activation of the endogenous kinases, as well as their predicted roles in cell cycle progression (3–6). It is unlikely that the effects are the result of nonspecific toxic effects because plasmids expressing the wild-type kinases gave no such change and could overcome the phenotype of the corresponding mutant. Therefore, we conclude that these mutants act in a dominant-negative fashion and create highly specific loss-of-function phenotypes.

If the effects of Cdk2 and Cdc2 mutants were the result of competition with the endogenous wild-type kinases for cyclin binding, the block should be overcome by overexpression of cyclins. Plasmids expressing cyclins A, B1, B2, C, D1, D3, and E

were transfected to test this possibility (26). Rescue of the Cdk2 dominant-negative effect was observed when a reduced amount of the mutant, resulting in a less stringent arrest, was transfected in a 1:2 ratio with the cyclin D1 plasmid (Fig. 2). Cyclins A and E were both less efficient in rescuing the inhibition, but their effectiveness was proportional to the level of their expres-

sion. No effects were observed when cyclins B1, B2, C, and D3 were cotransfected with the Cdk2 mutant. In contrast, a reduction of the Cdc2 dominant-negative effect was only observed when either cyclin B1 or B2 was coexpressed (27).

Although the rescue of Cdk2 and Cdc2 mutants by different cyclins points to specificity for G₁ versus mitotic cyclins, the

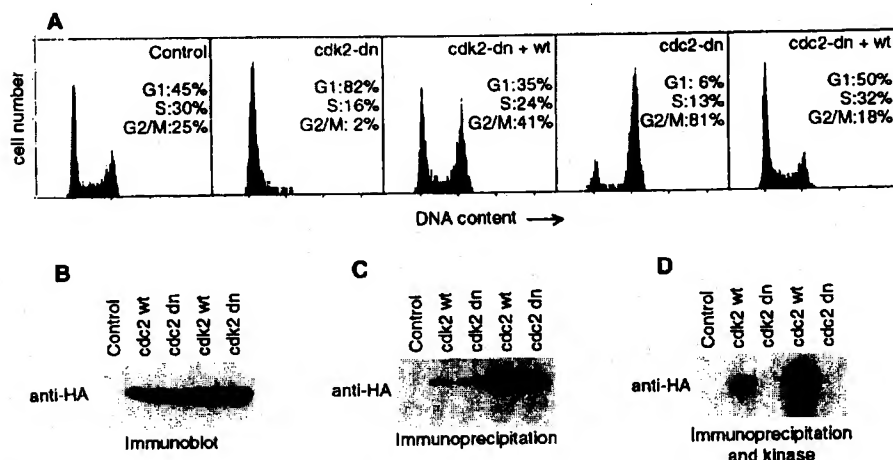
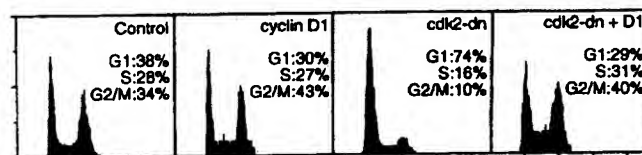


Fig. 1. Expression of mutant forms of Cdk2 and Cdc2 cause specific cell-cycle arrests. U2OS cells were transiently transfected with plasmids expressing the kinases indicated. Control cells are transfected with the CMV-neo-Bam vector. Dominant-negative (dn) and wild-type (wt) kinases were untagged in (A) whereas HA-tagged forms were expressed in (B), (C), and (D). (A) DNA histograms of CD20-positive cell populations in which relative DNA content is plotted against cell number. U2OS cells were transfected with 5 μ g of pCMVCD20 plus 20 μ g of CMV vector (control), 10 μ g of CMVcdk2-dn and 10 μ g of CMV vector (cdk2-dn), 10 μ g of CMVcdk2-dn and 10 μ g of CMVcdk2-wt (cdk2-dn + wt), 10 μ g of CMVcdc2-dn and 10 μ g of CMV vector (cdc2-dn), or 10 μ g of CMVcdc2-dn and 10 μ g of CMVcdc2-wt (cdc2-dn + wt). The cells were harvested 48 hours after the removal of DNA precipitates, stained for CD20 expression and DNA content, and analyzed by flow cytometry (33). (B) Expression levels of epitope-tagged mutant and wild-type Cdk2 and Cdc2 as determined by protein immunoblotting. Each lane contains 25 μ g of total lysate from cells transfected with 20 μ g of the CMV-neo-Bam vector (control) or 20 μ g of CMV plasmids expressing the indicated genes. Proteins were separated by SDS-PAGE (polyacrylamide gel electrophoresis), immunoblotted, and probed with the anti-HA monoclonal antibody 12CA5 as described (33). Similar results have been obtained with U2OS and C33A cells. To be able to compare expression levels of the different kinases, we used the same experiment and exposure for Fig. 3, B through D, and Fig. 4. (C) Immunoprecipitation of epitope-tagged mutant and wild-type Cdk2 and Cdc2. The anti-HA tag monoclonal antibody 12CA5 was used to immunoprecipitate ³⁵S-labeled proteins from U2OS cells transfected with the indicated plasmids. Medium was replaced 25 μ g of total lysate from cells transfected with 20 μ g of the CMV-neo-Bam vector (control) or 20 μ g of CMV plasmids expressing the indicated genes. Proteins were separated by SDS-PAGE (polyacrylamide gel electrophoresis), immunoblotted, and probed with the anti-HA monoclonal antibody 12CA5 as described (33). (D) In vitro histone H1 kinase activity associated with anti-HA immunoprecipitates. Transfections and immunoprecipitations were performed as in (C), but 200 μ g of total cellular protein was used for each immunoprecipitation, followed by incubation of the immunoprecipitates in kinase buffer supplemented with 4 μ g of histone H1 and 40- μ M [32P]ATP at 30°C for 30 min as described (8).

Fig. 2. Rescue of the Cdk2 dominant-negative phenotype by overexpression of cyclin D1. Saos-2 cells were transiently transfected with 2 μ g of the CMVCD20 plasmid in combination with 24 μ g of the CMV vector (control), 16 μ g of cyclin D1 plasmid and 8 μ g of the vector (D1), 8 μ g of CMVcdk2-dn and 16 μ g of vector (cdk2-dn), or 8 μ g of CMVcdk2-dn and 16 μ g of cyclin D1 plasmid. DNA histograms of CD20-positive Saos-2 cells are shown in which DNA content is plotted versus cell number as in Fig. 1. Cells were harvested 48 hours after the removal of DNA precipitates, stained, and analyzed by flow cytometry as in Fig. 1 and (22).



effect was highly dependent on the relative amount of the rescuing cyclin. Therefore, whereas the alleviation of the dominant-negative effects suggests that cyclin titration is at least part of the mechanism of inhibition, it does not necessarily reveal the cyclins that regulate the kinase *in vivo*. This restriction is substantiated by our inability to detect endogenous cyclin D1 in Saos-2 cells, although the Cdk2-dn effect could be rescued by cyclin D1 in these cells.

Because dominant-negative inhibition may uncover a requirement for other cyclin-dependent kinases in cell cycle progression, the corresponding Asp to Asn mutation was introduced into other candidate kinases, and both HA-tagged and -untagged forms were generated for each of the wild-type and mutant forms of these kinases. Plasmids expressing these kinases, driven by the CMV promoter, were transfected into several different human cell lines, and their expression and effects on cell cycle distribution were evaluated.

When the Cdk3 mutant was tested in these assays, it was also found to change the cell cycle profile (Fig. 3A), although its expression was found to be relatively low (Fig. 3D). The Cdk3 mutant resulted in an increased G₁ population in all 15 independent experiments in Saos-2 and C33A cells (mean \pm SD, 24.2% \pm 10.6%). Transfection of plasmids expressing wild-type Cdk3 did not have any noticeable effect.

We have supposed above that alteration of the flow cytometry profile by the dominant-negative mutants results from a block in cell cycle progression. However, another possibility is, in the case of Cdk3, that the mutant causes a G₁ increase as the consequence of the acceleration of S or G₂/M. To discriminate between these possibilities, we examined the effect of nocodazole on the Cdk3 dominant-negative phenotype. Nocodazole, which prevents spindle formation, causes cells that proceed through the cycle to accumulate in M phase. However, this drug should have no effect if the cells are already arrested in G₁. A substantial increase in the S and G₂/M populations was observed in control transfected cells when nocodazole was added 48 hours after transfection and cells were harvested 16 hours later. However, cells expressing the Cdk3-dn mutant did not accumulate in G₂/M (Fig. 3E). The lack of a nocodazole effect was specific for the Cdk3-dn- and CD20-positive cells because the same sample showed a large enrichment of cells at G₂/M when untransfected cells were included (Fig. 3E). Thus, the Cdk3 mutant causes a G₁ arrest and not acceleration of S or G₂/M.

Rescue experiments were performed to test the specificity of dominant-negative Cdk2 and Cdk3 because both mutants caused the accumulation of cells in G₁. The

amount of mutant plasmid was reduced to lower the dominant-negative effect and make rescue as sensitive as possible. Whereas wild-type Cdk2 could efficiently overcome the dominant-negative effect of the Cdk2 mutant, wild-type Cdk3 could not (Table 1). In the converse experiment, wild-type Cdk3 neutralized the effect of the Cdk3 mutant, but wild-type Cdk2 did not (Table 1). The fact that dominant-negative Cdk3 causes a G₁ block that can be rescued by wild-type Cdk3 suggests that Cdk3 func-

tion is required for G₁ progression.

The same increase in the G₁ population could be obtained with amounts of the Cdk3 mutant 1/10 to 1/20 that of the Cdk2 mutant (28). Because a relatively low amount of the Cdk3 mutant caused a dominant-negative phenotype, the endogenous amount of this kinase might be low. An affinity-purified rabbit antiserum raised against the 10 amino acids of the COOH-terminus of Cdk3 readily detected 36- and 33-kD proteins from Cdk3-transfected cells

Fig. 3. Dominant-negative Cdk3 is expressed at a relatively low level but causes the accumulation of cells in G₁. (A) Saos-2 cells were transiently transfected with 5 μ g of the CMVCD20 plasmid in combination with 20 μ g of the CMV vector (control), 20 μ g of CMVcdk2-dn (cdk2-dn), or 20 μ g of CMVcdk3-dn (cdk3-dn). DNA histograms of CD20-positive Saos-2 cells are depicted as in Figs. 1 and 2. The cells were harvested 48 hours after the removal of DNA precipitates, stained, and analyzed by flow cytometry (22). The expression levels of epitope-tagged mutant and wild-type Cdk2 and Cdk3 were determined by protein immunoblotting. Arrows indicate the position of Cdk2 and Cdk3 proteins. Each lane contains 25 μ g of total lysate from cells transfected with (B) 20 μ g of the CMV-neo-Bam vector (control), (C) 20 μ g of CMVcdk2-dn, or (D) 20 μ g of Cdk3-dn. Proteins were separated by SDS-PAGE, immunoblotted, and probed with the HA monoclonal antibody 12CA5. To compare expression levels of the different kinases, the same experiment and exposure is used for each panel, as in Fig. 1B and Fig. 4. (E) Cells expressing Cdk3-dn are blocked in G₁. Forty-eight hours after transfection, cells were refed with fresh medium (upper panel) or fresh medium containing nocodazole (NOC) (50 ng/ml; lower panel). The cells were harvested, stained, and analyzed by flow cytometry 16 hours later. Saos-2 cells were transfected with 3 μ g of CMVCD20 in combination with (left) 22 μ g of CMV vector or (middle and right) 22 μ g of CMVcdk3-dn. Left and middle histograms show the DNA content of the CD20-positive populations. Histograms at the right show the total population and include \geq 90% untransfected cells. The middle and right histograms are derived from the same samples.

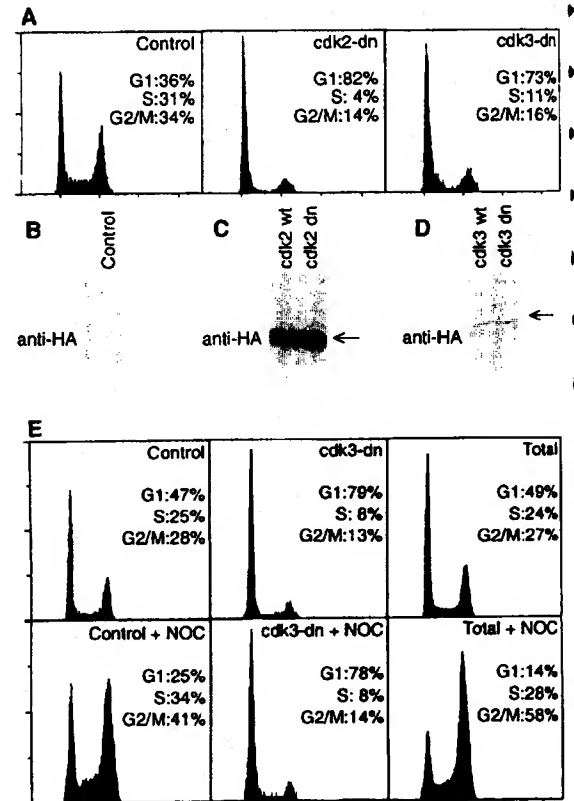


Table 1. Rescue of the Cdk2 and Cdk3 dominant-negative phenotype by coexpression of the corresponding wild-type kinases. Saos-2 cells were transiently transfected with 2 μ g of the CMVCD20 vector in combination with either 20 μ g of vector DNA or 10 μ g of each plasmid indicated below. The cell cycle profile of CD20-positive cells (percentage of cells in each stage) was determined by flow cytometry (22). Each value is the mean \pm SD of four independent experiments.

	Vector	Cdk2-dn + vector	Cdk2-dn + Cdk2-wt	Cdk2-dn + Cdk3-wt	Cdk3-dn + vector	Cdk3-dn + Cdk3-wt	Cdk3-dn + Cdk2-wt
G ₁	43 \pm 4	79 \pm 5	38 \pm 11	77 \pm 5	66 \pm 12	45 \pm 7	55 \pm 9
S	33 \pm 4	14 \pm 6	27 \pm 3	15 \pm 4	20 \pm 8	26 \pm 1	21 \pm 2
G ₂ /M	24 \pm 1	7 \pm 3	35 \pm 11	8 \pm 3	14 \pm 4	29 \pm 6	24 \pm 7

and proteins with the same mobility at much lower levels in untransfected normal human fibroblasts (W138) and human tumor cell lines (29). The expression of the Cdk3 proteins was roughly two orders of magnitude lower than that of Cdk2, as determined from the signal obtained when Cdk2 and Cdk3 immunoprecipitations were immunoblotted and probed with an anti-PSTAIRE monoclonal antibody. To date, we have been unable to detect cyclins associated with Cdk3 in experiments in which Cdk2- and Cdc2-associated cyclins were readily detected. However, cotransfection with cyclins D1 or E could largely overcome the dominant-negative Cdk3 effect, which is an indication that Cdk3 requires a cyclin partner for its function (27).

Transfection of plasmids encoding wild-type or mutant forms of Cdk4, Cdk5, Cdk6, and PCTAIRE-1 had no noticeable effect on the cell cycle distribution of transfected C33A, Saos-2, U2OS, or T98G cells (Fig. 4). Moderate (Cdk6) to very high levels of each kinase were found in transfected cells (Fig. 4). In several cases, we tested for redundancy by cotransfection of related kinases. For example, Cdk4 and Cdk6 share 71% identity in amino acid sequence (7); however, cotransfection of the Cdk4 and

Cdk6 mutants did not affect cell cycle distribution. Neither did combinations involving three or four of these mutant kinases. In this assay system, we cannot identify an essential role for the Cdk4, Cdk5, Cdk6, or PCTAIRE-1 kinases in cell cycle progression, but experiments in other systems will be required to evaluate such functions. Kinase activity associated with Cdk5 has been detected solely in terminally differentiated neuronal cells, suggesting that its function is unrelated to cell division (30).

Data from this and other studies suggest that different catalytic subunits have evolved in higher eukaryotes to control distinct cell cycle events (3–6). In addition to Cdc2 and Cdk2, Cdk3 appears to be one of such catalytic subunits. The phenotype of the dominant-negative Cdk3 mutant suggests that cellular Cdk3 executes a G_1 regulatory function. Several observations support this conclusion: (i) The effects of dominant-negative cyclin-dependent kinases were highly specific. The phenotypes of mutant Cdc2 and Cdk2 are distinct and consistent with their presumed functions, and mutant forms of several closely related kinases did not have any cell cycle effect. (ii) Coexpression of wild-type Cdk3 efficiently reversed the effect of mutant Cdk3. (iii) Growth arrest by dominant-negative

Cdk3 occurred at relatively low expression levels, in agreement with the low amount of the endogenous protein. (iv) Overexpression of G_1 cyclins can overcome the effect of dominant-negative Cdk3. (v) In previous work, Cdk3 was shown to be the only kinase in addition to Cdk2 and Cdc2 that could rescue yeast *cdc28* mutations (7). Together, our data suggest that the Cdk2 and Cdk3 kinases play essential and independent roles in G_1/S progression.

REFERENCES AND NOTES

1. L. H. Hartwell *et al.*, *Science* 183, 46 (1974); P. Nurse and Y. Bissett, *Nature* 292, 558 (1981); S. I. Reed and C. Wittenberg, *Proc. Natl. Acad. Sci. U.S.A.* 87, 5697 (1990).
2. G. Draetta, *Trends Biochem. Sci.* 15, 378 (1990); S. L. Forsburg and P. Nurse, *Annu. Rev. Cell Biol.* 7, 227 (1991); J. Pines and T. Hunter, *New Biol.* 2, 389 (1990).
3. F. Fang and J. W. Newport, *Cell* 66, 731 (1991).
4. J. P. Th'ng *et al.*, *ibid.* 63, 313 (1990); K. Riabowol *et al.*, *ibid.* 57, 393 (1989).
5. L.-H. Tsai, E. Lees, B. Faha, E. Harlow, K. Riabowol, *Oncogene* 8, 1593 (1993).
6. M. Pagano *et al.*, *J. Cell Biol.* 121, 101 (1993).
7. M. Meyerson *et al.*, *EMBO J.* 11, 2909 (1992).
8. L.-H. Tsai *et al.*, *Nature* 353, 174 (1991).
9. S. K. Hanks, *Proc. Natl. Acad. Sci. U.S.A.* 84, 388 (1987); J. Ninomiya-Tsuji, S. Nomoto, H. Yasuda, S. I. Reed, K. Matsumoto, *ibid.* 88, 9006 (1991); S. J. Elledge and M. R. Spottswood, *EMBO J.* 10, 2653 (1991); Y. Lapidot-Litson *et al.*, *Proc. Natl. Acad. Sci. U.S.A.* 89, 579 (1992).
10. Y. Xiong, H. Zhang, D. Beach, *Cell* 71, 505 (1992).
11. Abbreviations for the amino acid residues: A, Ala; C, Cys; D, Asp; E, Glu; F, Phe; G, Gly; H, His; I, Ile; K, Lys; L, Leu; M, Met; N, Asn; P, Pro; Q, Gln; R, Arg; S, Ser; T, Thr; V, Val; W, Trp; and Y, Tyr.
12. J. Pines and T. Hunter, *Nature* 346, 760 (1990); G. Draetta and D. Beach, *Cell* 54, 17 (1988); J. Pines and T. Hunter, *ibid.* 58, 833 (1989); J. Rosenblatt, Y. Gu, D. O. Morgan, *Proc. Natl. Acad. Sci. U.S.A.* 89, 2824 (1992); A. Koff *et al.*, *Science* 257, 1689 (1992); E. Lees, B. Faha, V. Dulić, S. I. Reed, E. Harlow, *Genes Dev.* 6, 1874 (1992); V. Dulić, E. Lees, S. I. Reed, *Science* 257, 1958 (1992); H. Matsushime *et al.*, *Cell* 71, 323 (1992).
13. M. Meyerson and E. Harlow, *Mol. Cell Biol.*, in press.
14. I. Herskowitz, *Nature* 329, 219 (1987).
15. S. K. Hanks, A. M. Quinn, T. Hunter, *Science* 241, 42 (1988).
16. S. S. Taylor *et al.*, *Trends Biochem. Sci.* 18, 84 (1993).
17. D. R. Knighton *et al.*, *Science* 253, 407 (1991); D. R. Knighton *et al.*, *ibid.*, p. 414; H. L. DeBordt *et al.*, *Nature* 363, 595 (1993).
18. M. D. Mendenhall, H. E. Richardson, S. I. Reed, *Proc. Natl. Acad. Sci. U.S.A.* 85, 4426 (1988).
19. B. Ducommun, P. Brambilla, G. Draetta, *Mol. Cell Biol.* 11, 6177 (1991); B. Ducommun *et al.*, *EMBO J.* 10, 3311 (1991).
20. Point mutations were introduced by in vitro mutagenesis. The DNA clones containing the open reading frames for each kinase were inserted into the Bam HI site of the pSelect vector (Promega), denatured, annealed to two different primers, and used for DNA synthesis, ligation, and transformation. One primer that contained a single mismatch in the middle was specific for each kinase and overlapped with most of the KLADFLG (11) encoding sequence. The DNA clones containing mutations were identified by DNA sequencing after a second transformation. A 7-amino acid epitope tag (YDVPDYA) was inserted just before the stop codon of each kinase, either by in vitro mutagenesis or by polymerase chain reaction (PCR). DNA sequencing was used to confirm the sequence of the tag. The complete open reading frame of the clones generated

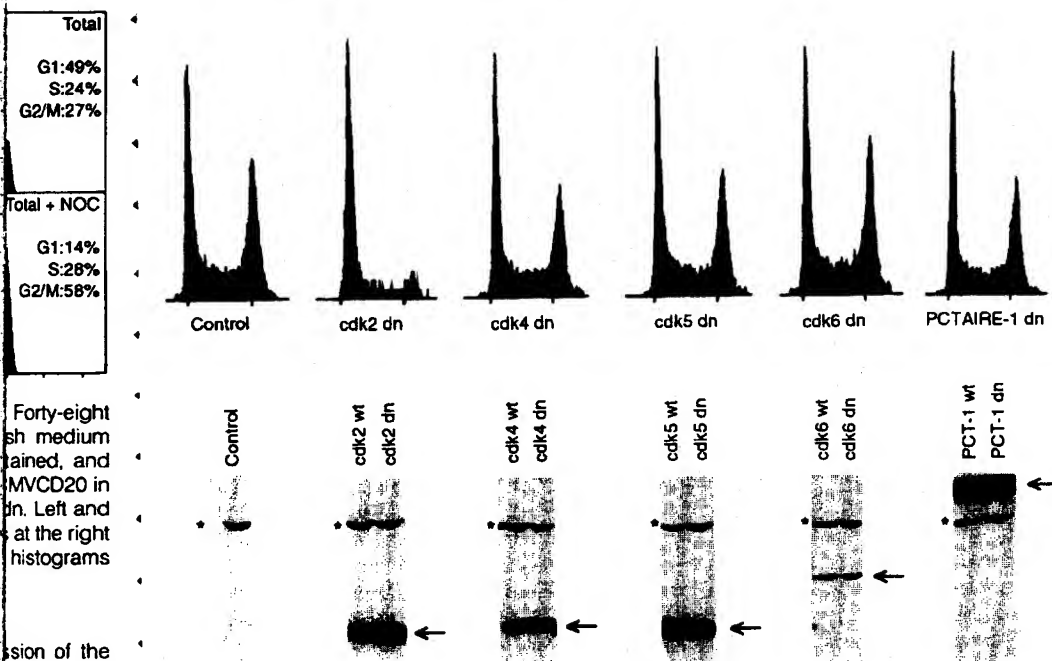


Fig. 4. Expression of mutant Cdk4, Cdk5, Cdk6, or PCTAIRE-1 (PCT-1) does not result in significant changes in cell cycle distribution. The top panel contains DNA histograms from CD20-positive C33A cells. DNA content is displayed versus cell number, as in Fig. 1. C33A cells were transiently transfected with 5 μ g of pCMVCD20 in combination with 20 μ g of plasmid DNA expressing the kinases indicated. The cells were harvested 48 hours after the removal of DNA precipitates, stained, and analyzed by flow cytometry (22). The lower panel shows the expression levels of epitope-tagged mutant and wild-type kinases as determined by protein immunoblotting. Arrows indicate the positions of each kinase. Asterisks indicate a cellular protein recognized by the 12CA5 antibody. Each lane contains 25 μ g of total lysate from transfected C33A cells. Proteins were separated by SDS-PAGE, immunoblotted, and probed with the anti-HA monoclonal antibody 12CA5. To compare expression levels of the different kinases, the same exposure was used for each panel, as in Figs. 1B and 3, B through D.

- by PCR was sequenced. The inserts were cloned into the Bam HI site of the CMV-neo-Bam vector (31) for expression in human cells.
21. For expression in *S. cerevisiae*, the coding regions of Cdc2 and Cdk2, mutant and wild-type and both tagged and untagged, were cloned into the Bam HI site of pMR438. The vector contains a GAL1 promoter upstream of the inserted genes, a yeast 2 μ origin of replication, and a URA3 selectable marker. All plasmids were tested in *S. cerevisiae* strain 10083-5C (MATa GAL cdc28-4 gcn4 ura3), and several were tested in K699 (MATa GAL cdc28-1N ade-1-1 can1-100 his3-11 leu2 trp1-1 ura3). Plasmids were transformed into yeast by the lithium acetate method and selected on plates lacking uracil and containing 2% glucose. Transformants were tested on plates containing either 2% glucose or 2% galactose at the permissive temperature (25°C) or nonpermissive temperature (36°C) as described (7).
 22. Cells were split 1:5 (Saos-2, C33A) or 1:8 (U2OS) and were transfected 20 hours later with calcium-phosphate precipitates of 20 to 26 μ g of plasmid DNA for each 100-mm dish (32). After 16 hours, the cells were washed twice with phosphate-buffered saline (PBS) and incubated with fresh medium (Dulbecco's minimum essential medium (DMEM) with 10% fetal bovine serum (FBS)). Forty-eight hours after the removal of DNA precipitates, cells were rinsed off the plates with PBS containing 0.1% EDTA, pelleted, and stained with 20 μ l of a fluorescein isothiocyanate (FITC)-conjugated anti-CD20 monoclonal antibody, as described (33). Subsequently, cells were washed twice and fixed overnight in 80% ethanol. Before analysis, the cells were pelleted, washed once, and stained in a solution of 20 μ g of propidium iodide and 250 μ g of ribonuclease (RNase) A per milliliter. Flow cytometry analysis was performed on a Becton-Dickinson FACScan, and data from 80,000 cells per sample were analyzed with the CellFIT Cell Cycle Analysis software. A gate was set to select CD20-positive cells with FITC staining at least 20 times stronger than that in the negative untransfected cells. Other gates were selected for single cells within a normal size range. The propidium iodide signal was used as a measure for DNA content and hence cell cycle stage. The DNA histograms each contain data from 1000 to 5000 CD20-positive cells.
 23. Associated cyclins were detected in re-immunoprecipitation experiments. We transfected U2OS cells with the tagged wild-type or mutant kinases and labeled them with ³⁵S-methionine. The HA-tag immunoprecipitations were denatured and re-immunoprecipitated with different anticyclin monoclonal antibodies.
 24. The DNA histograms of cells transfected with plasmids expressing the wild-type kinases were indistinguishable from controls transfected with the CMV vector.
 25. Expression of the Cdk2-dn mutant resulted in a G₁ arrest in all cell lines tested, including U2OS and Saos-2 osteosarcoma cells, C33A cervical carcinoma cells, T98G glioblastoma cells, and 293 human adenovirus-transformed kidney cells. The Cdc2-dn effect was most prominent in U2OS cells, and similar effects were seen in Saos-2 and T98G cells. However, the cell cycle distribution of C33A cells was not affected by this mutant. This latter result stresses that absence of a dominant-negative phenotype in this assay does not exclude a cell cycle function for the wild-type kinase in normal cells. Transformed cells may be resistant to dominant-negative inhibition, for example, as a result of overexpression of cyclins, activating kinase mutations or loss of growth-control pathways.
 26. P. W. Hinds *et al.*, *Cell* 70, 993 (1992).
 27. S. van den Heuvel and E. Harlow, unpublished data.
 28. We transfected Saos-2 cells with different amounts of the plasmids encoding HA-tagged mutant Cdk2 or Cdk3 and analyzed them by flow cytometry. Lysates from cells that showed equally increased G₁ populations were examined to quantitate the Cdk2-dn and Cdk3-dn protein levels. A serial dilution of the lysates (containing 0.2,

- 1, 5, or 25 μ g of protein) was separated by SDS-PAGE, immunoblotted, and probed with the 12CA5 antibody. The same G₁ increase appeared to be obtained with an amount of Cdk3-dn protein 1/10 to 1/20 of that of Cdk2-dn protein.
29. M. Meyerson and S. van den Heuvel, unpublished data.
30. J. Lew, R. J. Winkfein, H. K. Paudel, J. H. Wang, J. Biol. Chem. 267, 25922 (1992); L.-H. Tsai, T. Takahashi, V. S. Caviness Jr., E. Harlow, *Development*, in press.
31. S. J. Baker, S. Markowitz, E. R. Fearon, J. K. V. Willson, B. Vogelstein, *Science* 249, 912 (1990).
32. F. L. Graham and A. J. Van der Eb, *Virology* 52, 456 (1973); F. M. Ausubel *et al.*, Eds., *Current Protocols in Molecular Biology* (Wiley, New York, 1988), vol. 1.

33. L. Zhu *et al.*, *Genes Dev.* 7, 1111 (1993).
34. We thank D. Dombkowski for his help with the flow cytometry analysis, P. Hinds for the cyclin expression plasmids, I. Stamenkovic for the CD20 cDNA, G. Enders for the HA-tagged PCTAIRE-1 clone, and M. Vidal for help with the yeast experiments. M. Meyerson, L.-H. Tsai, E. Lees, K. Helin, J. Lees, and A. Fattaey are acknowledged for their careful reading of the manuscript. S.v.d.H. is a recipient of fellowships from the Netherlands Organization for Scientific Research (NWO) and the Helen Hay Whitney Foundation. E.H. is an American Cancer Society Research Professor and is supported by grants from the National Institutes of Health.

27 July 1993; accepted 20 October 1993

Receptive Field Reorganization in Dorsal Column Nuclei During Temporary Denervation

Michael J. Pettit and Harris D. Schwark*

Altered sensory input can result in the reorganization of somatosensory maps in the cerebral cortex and thalamus, but the extent to which reorganization occurs at lower levels of the somatosensory system is unknown. In cat dorsal column nuclei (DCN), the injection of local anesthetic into the receptive fields of DCN neurons resulted in the emergence of a new receptive field in all 13 neurons studied. New receptive fields emerged rapidly (within minutes), sometimes accompanied by changes in adaptation rates and stimulus selectivity, suggesting that the new fields arose from the unmasking of previously ineffective inputs. Receptive field reorganization was not imposed by descending cortical inputs to the DCN, because comparable results were obtained in 10 additional cells when the somatosensory and motor cortex were removed before recording. These results suggest that mechanisms underlying somatotopic reorganization exist at the earliest stages of somatosensory processing. Such mechanisms may participate in adaptive responses of the nervous system to injury or continuously changing sensory stimulation.

Sensory maps in the cerebral cortex are maintained through dynamic processes. Modification of peripheral inputs to the central nervous system results in reorganization of cortical somatosensory maps in a number of species (1) including humans (2). The identification of the mechanisms that are involved in map reorganization has clinical implications for the treatment of peripheral nerve injury and phantom limb pain.

A critical issue that must be resolved before the mechanisms of reorganization can be uncovered is the extent to which reorganization at subcortical levels contributes to changes previously described in the cortex. Mapping studies suggest that peripheral nerve transection can result in map reorganization in the primate ventral posterior thalamic nucleus (3). Such reorganization has not been found in DCN or trigeminal nuclei (4), although it is difficult to detect reorganization in subcortical maps, which are three-dimensional and can exhibit large somatotopic shifts over relatively

small distances. An alternative approach, which we have used in the present study, is to map a single neuron's receptive field, inject local anesthetic into the field to silence input from the receptive field temporarily, and then test for the appearance of a new receptive field. In thalamus (5) and cortex (6) this approach has been used to demonstrate that new receptive fields can emerge within minutes after the injection of lidocaine. Such changes in cat DCN neurons have not been investigated, although cold block of the dorsal columns has been reported to result in the emergence of new receptive fields in a small proportion of nucleus gracilis neurons (7).

To study subcortical reorganization in the present experiments, we recorded from 13 DCN neurons in six adult cats (8). Subcutaneous lidocaine injections into the original receptive field resulted in the rapid emergence of a new receptive field in every neuron tested (Table 1 and Fig. 1, A and B). However, the possibility remained that the primary site of reorganization was the cerebral cortex, and that subcortical reorganization was imposed by descending cortical inputs to the DCN. To test this possibility, we recorded from 10 neurons in four additional cats after the re-

Department of Biological Sciences, University of North Texas, Denton, TX 76203.

*To whom correspondence should be addressed.

Exhibit B

References Cited in Dr. Koshimizu's Declaration

Y. Daiaku, et al.

“Effect of Ischemic Preconditioning and Mitochondrial KATP Channel Openers on Chronic Left Ventricular Remodelin in the Ischemic-Reperfused Rat Heart”

Effect of Ischemic Preconditioning and Mitochondrial KATP Channel Openers on Chronic Left Ventricular Remodeling in the Ischemic-Reperfused Rat Heart

Yuka Dairaku, MD; Toshiro Miura, MD; Nozomu Harada, MD;
Masayasu Kimura, MD; Takayuki Okamura, MD; Hiroshi Iwamoto, MD;
Ryosuke Kametani, MD; Michio Yamada, MD; Yasuhiro Ikeda, MD;
Mitsuo Iwatate, MD; Shuji Kawamura, MD; Masunori Matsuzaki, MD

The influence of ischemic preconditioning (IP) and mitochondrial ATP-sensitive potassium (mito-KATP) channel openers on chronic left ventricular (LV) remodeling remains unknown, so the effect of IP and mito-KATP channel openers on the LV pressure–volume curve was assessed in rats subjected to 30 min ischemia followed by a 3-week reperfusion. Infarct size was histologically determined at 3 weeks after reperfusion. The LV pressure–volume curve was significantly shifted left by IP, diazoxide and nicorandil compared with the controls. These effects were blocked by the selective mito-KATP channel blocker 5-hydroxydecanoate. The LV remodeling and the infarct size at 3 weeks after reperfusion correlated well, indicating that the reduction of LV remodeling in the ischemic–reperfused model was strongly influenced by attenuation of the ischemic injury. LV remodeling in the chronic phase is attenuated by IP and mito-KATP channel openers with concomitant reduction of infarct size. (Circ J 2002; 66: 411–415)

Key Words: Diazoxide; Ischemic preconditioning; Nicorandil; Pressure–volume curve

A brief episode of ischemia–reperfusion reduces the size of the infarct caused by a subsequent longer ischemia–reperfusion insult. This phenomenon was first reported by Murry et al¹ and termed ischemic preconditioning (IP). The underlying mechanism of this phenomenon has been intensively investigated and one of the crucial mechanisms is the opening of the mitochondrial ATP-sensitive potassium (mito-KATP) channels.^{2–4} In order to mimic IP, the effect of mito-KATP channel openers has been investigated and these agents result in reduction of infarct size.^{5–12} However, the effect of IP and mito-KATP channel openers on chronic left ventricular (LV) remodeling has not been clarified yet. LV remodeling is a major determinant of prognosis after myocardial infarction¹³ and it may be determined by the infarct size and could be modified by drugs such as angiotensin-converting enzyme inhibitors.¹⁴ Thus, assessing LV remodeling is an important evaluation of whether or not interventions such as IP or mito-KATP channel openers are really effective. Furthermore, the reperfusion conditions, such as the no reflow phenomenon, may modify the infarct size and thus the LV remodeling in the chronic state. Therefore, the purpose of the present study was to investigate the effect of IP and mito-KATP channel openers on the extent of LV remodeling as assessed by the pressure–volume relationship, and to assess the correlation between infarct size and LV remodel-

ing during the chronic stage.

Methods

All experiments were performed in accordance with the Guide for the Care and Use of Laboratory Animals (NIH Publication No. 85-23) and were approved by the Animal Research Committee of Yamaguchi University School of Medicine.

Surgical Preparation

Male Sprague-Dawley rats (280–330 g) were anesthetized by intraperitoneal injection of sodium pentobarbital (60 mg/kg). Additional anesthesia was given during the experiment as required. After tracheal intubation, the rats were ventilated with a mixture of room air and 100% oxygen (respiratory rate, 65–70 breaths/min). After a thoracotomy in the fourth intercostal space, the heart was exposed and a thread was passed around the left anterior descending coronary artery (LAD) to occlude it. After 3 weeks of reperfusion, LV pressure (LVP) was measured by a 2F catheter-tip micromanometer (Model SPC-320, Millar Instruments, USA) inserted via the right carotid artery. The peak of the first derivative of LVP (+dP/dt) and the time constant of isovolumetric LVP decay (Tau) were calculated by an online data acquisition system (CODAS, DATAQ Instruments, Achon, OH, USA). The body temperature was maintained at 37±0.3°C by a heating pad.

Reagents

Diazoxide (Funakoshi, Osaka, Japan) was dissolved in dimethylsulfoxide (DMSO), the final concentration of which was less than 0.1%. Nicorandil (Chugai, Tokyo, Japan) was dissolved in saline at a concentration of 1.0

(Received October 26, 2001; revised manuscript received December 25, 2001; accepted January 9, 2002)

Department of Cardiovascular Medicine, Medical Bioregulation, Yamaguchi University School of Medicine, Ube, Japan
Mailing address: Masunori Matsuzaki, MD, The Division of Cardiovascular Medicine, Yamaguchi University, School of Medicine, 1-1-1 Minami-Kogushi, Ube 755-8505, Japan. E-mail: masunori@po.cc.yamaguchi-u.ac.jp

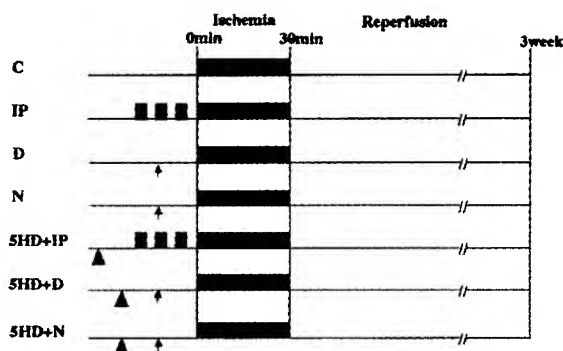


Fig 1. Rats were subjected to a 30-min coronary occlusion followed by 3 weeks of reperfusion in all groups ($n=6$, each). Ischemic preconditioning (IP) was performed by 3 cycles of 3 min of ischemia followed by 3 min of reperfusion. Diazoxide (3.5 mg/kg IV) and nicorandil (1.75 mg/kg IV) were administered 10 min before the 30-min ischemia (arrow). 5-hydroxydecanoate (5.0 mg/kg IV) was administered 10 min before IP or the infusion of diazoxide or nicorandil (arrowheads). C, controls; IP, ischemic preconditioning; D, diazoxide; N, nicorandil; 5HD, 5-hydroxydecanoate.

mg/ml. A selective mito-KATP channel inhibitor, 5-hydroxydecanoate (HD) (Sigma)^{2,9,15,16} was dissolved in saline.

Experimental Protocols

The experimental protocols are shown in Fig 1. Seven groups of rats ($n=6$, each) were subjected to 30 min ischemia created by occluding the LAD, followed by reperfusion for 3 weeks. IP was performed by 3 cycles of 3 min of ischemia followed by 3 min of reperfusion. Diazoxide (3.5 mg/kg IV) and nicorandil (1.75 mg/kg IV) were injected 10 min before the 30-min ischemia. 5-HD (5.0 mg/kg IV) was administered 10 min before either IP or diazoxide or nicorandil.

Quantitation of Infarct Size

Three weeks after the coronary reperfusion, the LAD was re-occluded and trypan blue dye (1.5%, 1 ml, Sigma Chemical, Co, St Louis, MO, US) was injected into the ascending aorta to delineate the risk and non-risk area in the hearts. The hearts were then excised and sliced into sections approximately 1 mm in width. Each slice was imaged by a color CCD camera (FV-10, Fuji, Japan), and the images were analyzed by image analyzing software (NIH image). The area unstained by the blue dye is the area at risk. The heart was fixed in 10% phosphate-buffered formalin, processed and embedded in paraffin. Transverse sections (4 μ m) were stained by the modified azan staining. The area of infarction was identified histologically and the infarct

size expressed as a percentage of the area at risk.

Pressure–Volume Relation

According to the method of Pfeffer et al,¹⁷ the in vitro LV pressure–volume curve was measured. In brief, the heart was arrested by an infusion of KCl and then quickly excised. A double-lumen catheter was inserted into the left ventricle, which was isolated by ligating the atrioventricular groove. The right ventricle was incised to eliminate the compressive effect. The left ventricle was emptied by evacuation through the catheter with manual compression. Reproducible pressure–volume curves were generated over a pressure range of 10–30 mmHg by infusing saline at a speed of 0.6 ml/min. These procedures were performed within 10 min of cardiac arrest and before the onset of rigor mortis. The volume index (volume/body weight) of the respective LVP at 10, 20 and 30 mmHg was assessed.

Statistical Analysis

All values are expressed as the mean \pm SE. Differences in hemodynamic parameters among the groups were analyzed by 2-way ANOVA. Fisher's test was used when a significant F value was obtained. Inter-group differences in area at risk, infarct size and left ventricular volumes of pressure–volume curves were analyzed by 1-way ANOVA followed by Fisher's test. Correlation between infarct size and the extent of LV remodeling was expressed as LV volume index (volume/body weight) at LVP of 20 mmHg was assessed by linear regression analysis with comparison of the 2 regression parameters of slope and intercept. Differences were considered significant at $p<0.05$.

Results

Hemodynamic Responses

Hemodynamic data at 3 weeks after reperfusion are presented in Table 1. Heart rate, peak LVP, end-diastolic LVP, (+)dP/dt, and Tau were not significantly different among the groups.

Infarct Size

In the acute phase, 15% of animals died of technical problems such as pneumothorax and bleeding, but no death from heart failure occurred. In the chronic phase, no deaths occurred. Risk area was not statistically different among the groups (Fig 2A). As shown in Fig 2B, infarct size was significantly reduced by IP (16 \pm 1%, $p<0.01$ vs controls), compared with the controls (72 \pm 4%), and by both diazoxide (40 \pm 4%, $p<0.05$ vs controls) and nicorandil (28 \pm 2%, $p<0.01$ vs controls). The effect of IP, diazoxide and nico-

Table 1 Hemodynamics After 3-Weeks of Reperfusion

	HR (beats/min)	Peak LVP (mmHg)	LVEDP (mmHg)	(+)dP/dt (mmHg/s)	Tau (ms)
C	395 \pm 17	113 \pm 1	5 \pm 4	7,721 \pm 768	12 \pm 1
IP	410 \pm 5	115 \pm 7	7 \pm 2	6,215 \pm 1,207	14 \pm 1
D	440 \pm 5	97 \pm 1	4 \pm 1	7,643 \pm 377	10 \pm 1
N	395 \pm 11	98 \pm 3	4 \pm 1	8,228 \pm 524	10 \pm 1
5HD+IP	378 \pm 5	90 \pm 2	4 \pm 2	7,015 \pm 196	12 \pm 1
5HD+D	419 \pm 10	96 \pm 7	9 \pm 3	7,270 \pm 731	17 \pm 3
5HD+N	430 \pm 11	98 \pm 6	5 \pm 1	8,158 \pm 834	11 \pm 1

HR, heart rate; LVP, left ventricular pressure; LVEDP, left ventricular end-diastolic pressure; (+)dP/dt, maximum rate of LVP generation; Time constant, time constant of the LVP fall during isovolumic relaxation period. Other abbreviations are the same as in Fig 1. Values are mean \pm SE. $N=6$, each.

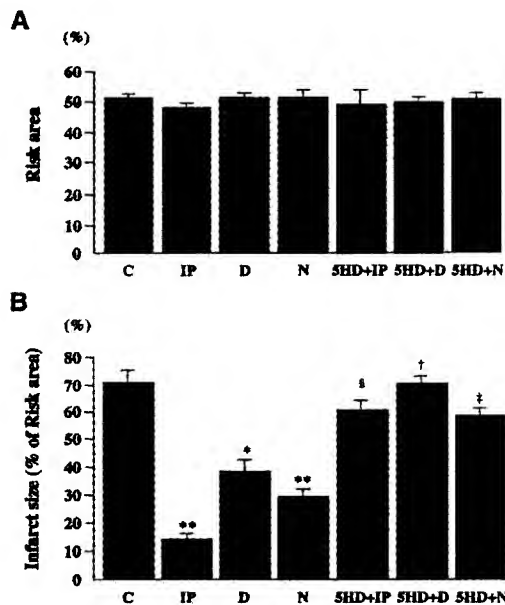


Fig2. (A) The risk area was identical in all groups. (B) Infarct size was reduced by IP, D, and N compared with C. The effect of IP, D and N was abolished by 5-HD. * $p < 0.05$ vs C, ** $p < 0.01$ vs C, $^{\dagger}p < 0.05$ vs IP, $^{\ddagger}p < 0.05$ vs D, $^{\S}p < 0.05$ vs N. All abbreviations as in Fig 1.

randil on infarct size was inhibited by 5-HD ($61 \pm 2\%$ $p < 0.05$ vs IP, $72 \pm 3\%$ $p < 0.05$ vs diazoxide, $60 \pm 2\%$ $p < 0.05$ vs nicorandil).

In Vitro LV Pressure–Volume Relation

The in vitro LV pressure–volume curve shifted left with IP compared with the controls (Fig3). With diazoxide or nicorandil, the pressure–volume curve also significantly shifted left compared with the controls. Indeed, the left shift of the LV pressure–volume curve by IP, diazoxide or nicorandil was abolished by 5-HD.

Correlation Between the Infarct Size and LV Remodeling

Linear regression analysis revealed a good correlation between the infarct size (% of area at risk) and the extent of LV remodeling expressed as the LV volume index (volume/body weight) at a LVP of 20 mmHg. The slope of the correlation was 0.014 ($r = 0.78$, $p < 0.001$) (Fig4).

Discussion

One of the major findings of the present study is that IP attenuates LV remodeling concomitant with a reduction in infarct size in the chronic stage. Although the reduction of infarct size by IP has been demonstrated in the acute phase (ie, 4–6 h after the reperfusion determined by TTC staining)^{2,18–23} it has not been clear whether IP attenuates LV remodeling. Our study is the first to demonstrate that LV remodeling was attenuated by IP according to the reduction of the size of the histologically determined infarct. Cohen et al showed an improvement in the function of the ischemic myocardium 24 h after reperfusion in a rabbit model of ischemia–reperfusion²⁴ However, they focused only on the ischemic area, and the change in the remote area was not determined. Our study clearly showed that using pressure–volume relation the whole LV chamber remodeling was estimated.

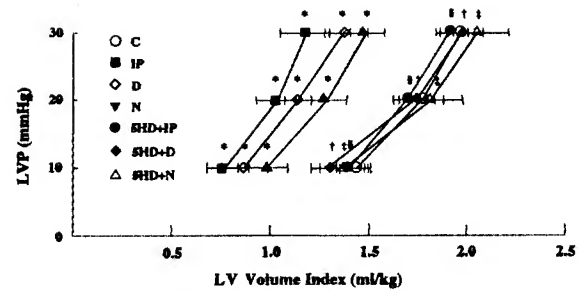


Fig3. The left ventricular pressure–volume curve was significantly shifted leftward by IP, D, and N compared with C. The shift in the curve caused by IP, D and N was abolished by 5HD ($n = 6$ each). Data are shown as mean \pm SE. * $p < 0.05$ vs C, $^{\dagger}p < 0.05$ vs IP, $^{\ddagger}p < 0.05$ vs 5HD+D, $^{\S}p < 0.05$ vs the 5HD+N. All abbreviations as in Fig 1.

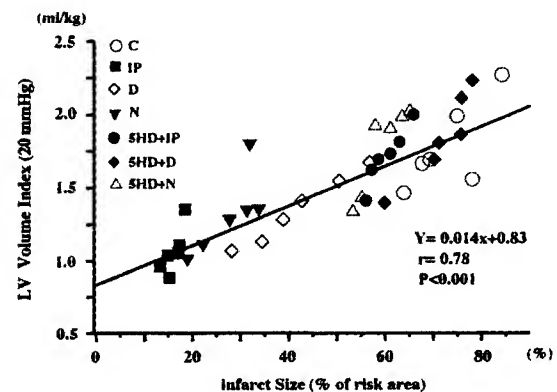


Fig4. Linear regression analysis revealed a good correlation between the infarct size (% of area at risk) and the extent of remodeling expressed as LV volume (ml/kg) at LV pressure of 20 mmHg. The slope of the correlation is 0.014 ($r = 0.78$, $p < 0.001$). All abbreviations as in Fig 1.

The infarct size determined by TTC staining correlates with the histologically determined infarct in the permanent coronary occlusion model²⁵ However, in the ischemia–reperfusion model, the infarct size in the chronic stage may be influenced by the perfusion conditions; the no-reflow phenomenon increases the infarct size in the chronic stage in large animals and humans^{26–28} and Shimizu et al demonstrated that no-reflow occurs in the isolated rat heart²⁹ Furthermore, no-reflow is demonstrated in the skeletal muscle in rat and that is attenuated by IP³⁰ So, the effect of IP or drugs on infarct size may differ between the acute and chronic stages. The infarct size may be determined within 6 h of reperfusion, but it should be taken into consideration that the infarct size determined by TTC after 6 h of reperfusion was smaller than that determined histologically at 3 weeks in the control group ($60 \pm 2\%$ vs $72 \pm 4\%$), and in the IP group the size of the infarct at 3 weeks was smaller than that after 6 h of reperfusion ($16 \pm 1\%$ vs $26 \pm 2\%$)³¹ This suggests that infarct size may be influenced by the reflow conditions.

It has been shown that attenuation of LV remodeling is a major determinant of survival after acute myocardial infarction although its underlying mechanism is not well understood^{13,32} Pfeffer et al showed that captopril attenuated LV dilatation after myocardial infarction in a permanent coronary occlusion model^{33,34} In their study, infarct

size was identical in the control and captopril groups, so extension of the non-ischemic myocardium was inhibited by captopril. In the present study, the infarct size was diminished by IP, thus the reduction in infarct size strongly influenced the extent of LV remodeling. Fig 4 shows the correlation between the extent of LV remodeling, which was expressed as the LV volume index of LVP at 20 mmHg, and the infarct size. Because we used IP and KATP openers to reduce infarct size, we cannot totally exclude that possibility that it is not only the infarct size–LV volume index relationship shown in Fig 4. However, IP and injection of KATP openers were performed only once before sustained ischemia and it has been shown that the topography of myocardial salvage does not differ between earlier reperfusion, IP and KATP openers. Therefore, it is likely that the relationship in Fig 4 is applicable to infarct size limitation by the earlier reperfusion. Nevertheless, a good correlation between the infarct size and LV volume index indicates that the infarct size is the most important determinant of LV remodeling in the ischemic–reperfused heart.

In the present study, the hemodynamic measurement at 3 weeks after reperfusion demonstrated that the LV end diastolic pressure was not elevated in all groups, in spite of the difference in infarct size. This result indicates that the compensation of the LV to the loss of myocardium was fully exerted. The LV remodeling may be a compensated process in this model and the lesser remodeling indicates attenuation of myocardial damage. It is important to consider where the myocardium is remodeled. In the ischemic–reperfused model, there are 3 types of LV myocardium: the non-ischemic, ischemic but viable, and infarcted regions. As has been shown, the infarcted region becomes a scar and usually shrink in 3 weeks. Thus, it is the ischemic but viable myocardium and the non-ischemic myocardium that play an important role in the remodeling, but how much each region affects the remodeling process could not be determined from the data in the present study. This should be further investigated.

The second of the major findings is that the mito-KATP channel openers, diazoxide and nicorandil, can mimic the effect of IP in terms of ventricular remodeling as well as reduction of infarct size. Because the selective blockade of the mito-KATP channels by 5-HD abolished the effect of diazoxide and nicorandil on both infarct size and LV remodeling, the opening of the mito-KATP channels is a crucial mechanism in the reduction of infarct size and attenuation of LV remodeling. The major mechanism of these drugs is the reduction in infarct size as demonstrated by the correlation in Fig 4.

Diazoxide has more effect on the mito-KATP channels than the sarcolemmal KATP channels³⁵ and it also acts strongly on the arterial smooth muscle KATP channels, which dilate the arterioles and cause systemic hypotension.³⁶ Recent evidence shows that the vascular smooth muscle KATP channels are composed of Kir6.1 or 6.2 with SUR2B subunits and that the cardiomyocyte sarcolemmal KATP channels consist of Kir6.2 with SUR2A subunits.^{37,38} Diazoxide is a potent K⁺ channel-opening drug for constructed SUR1/Kir6.2 and SUR2B/Kir6.2 channels, but not for the SUR2A/Kir6.2 channel.³⁹ The dose of diazoxide we used was almost the maximum that could be used in an *in vivo* study.

Nicorandil acts on both sarcolemmal and mito-KATP channels,⁴⁰ and also has a nitrate effect.⁴¹ The effect of diazoxide was completely blocked by 5-HD, but its effect

on nicorandil was not complete, as shown by Fig 4. This may be attributed to its combined effect, although it was small in the present study. However, Sanada et al showed that in a dog model, the sarcolemmal and mito-KATP channels were equally important in reducing infarct size.⁹ The species difference should be noted and we should be careful in extrapolating the data to humans. Recently it has been shown that nitric oxide accelerates the mito-KATP channel opening,⁴² and it may be the nitric oxide effect of nicorandil that accelerates the mito-KATP channel opening. It remains to be determined how important this effect of nicorandil is on the opening of mito-KATP channels.

We conclude that chronic LV remodeling after an ischemia–reperfusion insult was suppressed by IP and by mito-KATP channel openers, with a concomitant reduction of the size of the histologically determined infarct after 3 weeks of reperfusion.

Acknowledgments

This study was supported in part by research grant from the Ministry of Education, Science and Culture of Japan. We wish to thank Ms Rie Ishihara and Ms Kazuko Iwamoto for their excellent technical assistance.

References

1. Murry CE, Jennings RB, Reimer KA. Preconditioning with ischemia: A delay of lethal cell injury in ischemic myocardium. *Circulation* 1986; **74**: 1124–1136.
2. Auchampach JA, Grover GJ, Gross GJ. Blockade of ischemic preconditioning in dogs by the novel ATP dependent potassium channel antagonist sodium 5-hydroxydecanate. *Cardiovasc Res* 1992; **26**: 1054–1062.
3. Baker JE, Holman P, Gross GJ. Preconditioning in immature rabbit hearts: Role of KATP channels. *Circulation* 1999; **99**: 1249–1254.
4. Fryer RM, Eells JT, Hsu AK, Henry MM, Gross GJ. Ischemic preconditioning in rats: Role of mitochondrial KATP channel in preservation of mitochondrial function. *Am J Physiol* 2000; **278**: H305–H312.
5. Garlid KD, Paucek P, Yarov-Yarovsky V, Murray HN, Darbenzio RB, D'Alonzo AJ, et al. Cardioprotective effect of diazoxide and its interaction with mitochondrial ATP-sensitive K⁺ channels. *Circ Res* 1997; **81**: 1072–1082.
6. Garlid KD, Paucek P, Yarov-Yarovsky V, Sun X, Schindler PA. The mitochondrial KATP channel as a receptor for potassium channel openers. *J Biol Chem* 1996; **271**: 8796–8799.
7. Gross GJ, Fryer RM. Sarcolemmal versus mitochondrial ATP-sensitive K⁺ channels and myocardial preconditioning. *Circ Res* 1999; **84**: 973–979.
8. Liu Y, Sato T, O'Rourke B, Marban E. Mitochondrial ATP-dependent potassium channels, novel effectors of cardioprotection? *Circulation* 1998; **97**: 2463–2469.
9. McCullough JR, Normandin DE, Conder ML, Sleph PG, Dzwonczyk S, Grover GJ. Specific block of the anti-ischemic actions of cromakalim by sodium 5-hydroxydecanate. *Circ Res* 1991; **69**: 949–958.
10. Sato T, Sakai N, O'Rourke B, Marban E. Nicorandil, a potent cardioprotective agent, acts by opening mitochondrial ATP-dependent potassium channels. *J Am Coll Cardiol* 2000; **35**: 514–518.
11. Wu DJ, Minatoguchi S, Uno Y, Arai M, Wang N, Nishida Y, et al. Combination of N-methyl-L-deoxyojirimycin and ischemic preconditioning markedly reduces the size of myocardial infarcts in rabbits. *Jpn Circ J* 2001; **65**: 673–677.
12. Yasuda T, Hashimura K, Matsu-ura Y, Kato Y, Ueda T, Mori I, et al. Nicorandil, a hybrid between nitrate and ATP-sensitive potassium channel opener, preconditions human heart to ischemia during percutaneous transluminal coronary angioplasty. *Jpn Circ J* 2001; **65**: 526–530.
13. Chareonthaitawee P, Christian TF, Hirose K, Gibbons RJ, Rumberger JA. Relation of initial infarct size to extent of left ventricular remodeling in the year after acute myocardial infarction. *J Am Coll Cardiol* 1995; **25**: 567–573.
14. Lee KS, Marwick TH, Cook SA, Go RT, Fix JS, James KB, et al. Prognosis of patients with left ventricular dysfunction, with and without viable myocardium after myocardial infarction: Relative efficacy of medical therapy and revascularization. *Circulation* 1997;

- 90: 2687–2694.
15. Jaburek M, Yarov-Yarovoy V, Paucek P, Garlid KD. State-dependent inhibition of the mitochondrial K_{ATP} channel by glyburide and 5-hydroxydecanoate. *J Biol Chem* 1998; **273**: 13578–13582.
 16. Joyeux M, Godin-Ribuot D, Ribaut C. Resistance to myocardial infarction induced by heat stress and the effect of ATP-sensitive potassium channel blockade in the rat isolated heart. *Br J Pharmacol* 1998; **123**: 1085–1088.
 17. Pfeffer JM, Pfeffer MA, Fletcher PJ, Braunwald E. Progressive ventricular remodeling in rat with myocardial infarction. *Am J Physiol* 1991; **260**: H1406–H1414.
 18. Cohen MV, Yang Xi-M, Downey JM. Smaller infarct after preconditioning dose not predict extent of early functional improvement of reperfused heart. *Am J Physiol Heart* 1999; **277**: H1754–H1761.
 19. Miura T, Liu Y, Kita H, Ogawa T, Shimamoto K. Role of mitochondrial ATP-sensitive K⁺ channels and PKC in anti-infarct tolerance afforded by adenosine A₁ receptor activation. *J Am Coll Cardiol* 1999; **35**: 238–245.
 20. Sanada S, Kitakaze M, Asanuma H, Harada K, Ogita H, Node K, et al. Role of mitochondrial and sarcolemmal K_{ATP} channels in ischemic preconditioning of canine. *Am J Physiol* 2001; **280**: H256–H263.
 21. Schultz JEJ, Hsu AK, Gross GJ. Ischemic preconditioning in the intact rat heart is mediated by σ 1 but not μ - or κ -opioid receptors. *Circulation* 1998; **97**: 1282–1289.
 22. Wang Y, Hirai K, Ashraf M. Activation of mitochondrial ATP-sensitive K⁺ channel for cardiac protection against ischemic injury is dependent on protein kinase C activity. *Circ Res* 1999; **85**: 731–741.
 23. Fishbein MC, Meerbaum S, Rit J, Lando U, Kanmatsuse K, Mercier Jc, et al. Early phase acute myocardial infarct size quantification: Validation of the triphenyl tetrazolium chloride tissue enzyme staining technique. *Am Heart J* 1981; **101**: 593–600.
 24. Cohen MV, Yang Xi-M, Neumann T, Heusch G, Downey JM. Favorable remodeling enhances recovery of regional myocardial function in the weeks after infarction in ischemically preconditioned hearts. *Circulation* 2000; **102**: 579–583.
 25. Zardini P, Marino P, Golia G, Anselmi M, Castelli M. Ventricular remodeling and infarct expansion. *Am J Cardiol* 1993; **72**: 98–106.
 26. Morishima I, Sone T, Okumura K, Tsuboi H, Kondo J, Mukawa H, et al. Angiographic no-reflow phenomenon as a predictor of adverse long-term outcome in patients treated with percutaneous transluminal coronary angioplasty for first acute myocardial infarction. *J Am Coll Cardiol* 2000; **36**: 1202–1209.
 27. Sakata Y, Kodama K, Komamura K, Lim YJ, Ishikura F, Hirayama A, et al. Salutary effect of adjunctive intracoronary nicorandil administration on restoration of myocardial blood flow and functional improvement in patients with acute myocardial infarction. *Am Heart J* 1997; **133**: 616–621.
 28. Iwakura K, Ito H, Kawano S, Shintani Y, Yamamoto K, Kato A, et al. Predictive factors for development of the no-reflow phenomenon in patients with reperfused anterior wall acute myocardial infarction. *J Am Coll Cardiol* 2001; **38**: 472–477.
 29. Shimizu M, Wang QD, Sjoquist PO, Rydem L. The angiotensin II AT₁-receptor antagonist candesartan improves functional recovery and reduces the no-reflow area in reperfused ischemic rat hearts. *J Cardiovasc Pharmacol* 1999; **34**: 78–81.
 30. Wang WZ, Anderson G, Firrell JC, Tsai TM. Ischemic preconditioning versus intermittent reperfusion to improve blood flow to a vascular isolated skeletal muscle flap of rats. *J Trauma* 1998; **45**: 953–959.
 31. Okamura T, Miura T, Iwamoto H, Shirakawa K, Kawamura S, Ikeda Y, et al. Ischemic preconditioning attenuates apoptosis through protein kinase C in rat hearts. *Am J Physiol* 1999; **277**: H1997–H2001.
 32. White HD, Norris RM, Brown MA, Brandt PWT, Whitlock RML, Wild CJ. Left ventricular end-systolic volume as the major determinant of survival after recovery from myocardial infarction. *Circulation* 1987; **76**: 44–51.
 33. Pfeffer MA, Pfeffer JM, Steinberg C, Finn P. Survival after an experimental myocardial infarction: Beneficial effects of long-term therapy with captopril. *Circulation* 1985; **72**: 406–412.
 34. Pfeffer MA, Braunwald E, Myoe LA, Basta L, Brown EJ Jr, Cuddy TE, et al. On behalf of the SAVE investigators. Effect of captopril on mortality and morbidity in patients with left ventricular dysfunction after myocardial infarction: Result of the survival and ventricular enlargement trial. *N Engl J Med* 1992; **327**: 669–677.
 35. Sato T, Sasaki N, Seharaseyon J, O'Rourke B, Marban E. Selective pharmacological agents implicate mitochondrial but not sarcolemmal K_{ATP} channels in ischemic cardioprotection. *Circulation* 2000; **101**: 2418–2423.
 36. Powell WJ, Green RM, Whiting RB, Sanders CA. Action of diazoxide on skeletal muscle vascular resistance. *Circ Res* 1971; **28**: 167–178.
 37. Yokoshiki H, Sunagawa M, Seki T, Sperelakis N. ATP-sensitive K⁺ channels in pancreatic, cardiac, and vascular smooth muscle cells. *Am J Physiol* 1998; **274**: C25–C37.
 38. Pluja L, Yokoshiki H, Sperelakis N. Evidence for presence of ATP-sensitive K⁺ channels in rat colonic smooth muscle cells. *Can J Physiol Pharmacol* 1998; **76**: 1166–1170.
 39. Yokoshiki H, Sunagawa M, Seki T, Sperelakis N. Antisense oligodeoxynucleotides of sulfonyleurea receptors inhibit ATP-sensitive K⁺ channels in cultured neonatal rat ventricular cells. *Pflügers Arch* 1999; **437**: 400–408.
 40. Davie CS, Kubo M, Standen NB. Potassium channel activation and relaxation by nicorandil in rat small mesenteric arteries. *Br J Pharmacol* 1998; **125**: 1715–1725.
 41. Pieper GM, Gross GJ. Salutary action of nicorandil, a new antianginal drug, on myocardial metabolism during ischemia and on postischemic function in a canine preparation of brief, repetitive coronary artery occlusions; comparison with isosorbide dinitrate. *Circulation* 1987; **76**: 916–928.
 42. Sasaki N, Sato T, Ohler A, O'Rourke B, Marban E. Action of mitochondrial ATP-dependent potassium channels by nitric oxide. *Circulation* 2000; **101**: 439–445.

Exhibit B

References Cited in Dr. Koshimizu's Declaration

P.J. O'Brien, et al.

**"Cardiac Troponin T is a Sensitive, Specific
Biomarker of Cardiac Injury in laboratory Animals"**

Cardiac Troponin T is a Sensitive, Specific Biomarker of Cardiac Injury in Laboratory Animals

Peter J. O'Brien,^{1*} Gregory W. Dameron,¹ Mary Lee Beck,¹ Y. James Kang,²
B. Kipp Erickson,³ Tana H. Di Battista,³ Kim E. Miller,³ Keith N. Jackson,⁴ and Scott Mittelstadt⁴

Abstract | A reliable serum assay that can discriminate between cardiac and skeletal muscle injury is not available for diagnostic use in laboratory animals. We tested and supported the hypotheses that serum cardiac troponin T (cTnT) was widely applicable in laboratory animals as a biomarker of cardiac injury arising from various causes; that it increased in proportion to severity of cardiac injury; and that it was more cardiospecific than creatine kinase (CK) or lactate dehydrogenase (LD) isozyme activities. In canine and rat models of myocardial infarction, cTnT concentration increased 1,000- to 10,000-fold and was highly correlated with infarct size within 3 h of injury. Serum CK and LD isozymes were substantially less effective biomarkers and, in contrast to cTnT, were ineffective markers in the presence of moderate skeletal muscle injury, with resulting serum CK activity >5,000 U/L. Using these animal models, and mouse and ferret models, we also showed cTnT to be an effective biomarker in doxorubicin cardiotoxicosis, traumatic injury, ischemia, and cardiac puncture. Reference range serum concentrations for all species were at the detection limit of the assay, except those for mice, in which they were slightly increased, possibly because mice were used to generate assay monoclonal antibodies. We conclude that cTnT is a powerful biomarker in laboratory animals for the sensitive and specific detection of cardiac injury arising from various causes.

To the authors' knowledge, there is no serum assay that can discriminate between cardiac and skeletal muscle injury in laboratory animals. Electrophoretic tests for isozymes of creatine kinase (CK) and lactate dehydrogenase (LD) have been used effectively for detection of myocardial infarction in people. However, their use in laboratory animals for detection of cardiac injury is complicated by several factors. These tests are recognized as having restricted specificity and sensitivity for medical use in detection of cardiac injury (1).

Blood tests for cardiac injury that are based on electrophoretic determination of serum CK or LD isozyme activity may yield false-negative results in some species more frequently than when these tests are used in people. For example, in swine, rabbits, and horses, activity of the myocardial CK isozyme is undetectable or low (2-4). Also, complication of cardiac injury by skeletal muscle injury is more likely in animals than in people. Mild or moderate muscle injury frequently occurs with exertion, bruising, or stress during animal handling, especially in wild or laboratory animals. This may cause increased release of skeletal muscle CK and LD isozymes that obscure detection of in-

creased activity of cardiac isozymes (CK-MB, LD-1, LD-2) (4). Furthermore, in some species with high serum albumin concentration (e.g., rats), serum CK-MB activity may be obscured by co-migration of albumin fluorescence (5). Finally, similar to that in people, the relatively slow release of LD (1 to 2 days) and rapid clearance of CK (1 to 3 days) from the blood restricts the time interval after injury during which these biomarkers may be useful (6).

False-positive test results for cardiac injury, based on electrophoretic determination of serum CK or LD isozyme activity, also may be obtained because these isozymes are not found exclusively in the heart. Slow-twitch or endurance-trained skeletal muscle fibers contain higher content of cardiac isozymes of CK and LD than do fast-twitch or untrained muscle fibers (7). In contrast to human beings, hepatic LD-1 and LD-2 activities are high in cattle, horses, and swine. Consequently, hepatocellular injury causes a false-positive LD isozyme test result for cardiac injury in these species (4, 6). Furthermore, platelet or erythrocyte lysis releases CK and LD, which may be of the cardiac type in some species (8, 9).

Recently, assays have been developed for the specific and sensitive detection of myocardial infarction in people (1, 10). Most of these assays are based on immunologic detection of a protein, such as cardiac troponin T (cTnT), gene expression of which is restricted to striated muscle, principally cardiac muscle. Compared with LD, this protein is released relatively rapidly into the blood, and compared with LD and CK, it is more persistent in the blood (1, 10).

Troponin T is a myofibrillar protein that is important in

Human Safety Department, The Procter and Gamble Company, Cincinnati, Ohio¹; Department of Medicine, University of Louisville, Louisville, Kentucky²; Procter and Gamble Pharmaceuticals, Norwich, New York³; Procter and Gamble Pharmaceuticals, Health Care Research Center, Mason, Ohio⁴

*Address correspondence to Dr. Peter J. O'Brien, Clinical Laboratory Medicine, Safety Assessment - UK, SmithKline Beecham Pharmaceuticals, The Frythe, Welwyn, Hertfordshire, U.K. AL6 9AR.

regulating striated muscle contraction. Its structure has been highly conserved across phyla (11). The cTnT immunoassay used for detection of myocardial injury in people detects blood activity in various species of animals after various types of cardiac injury: in rats after toxic (12), ischemic (13), and immunologic (14) injury to myocardium; in mice with myocarditis (15); in dogs after ischemic myocardial injury (16); and in broiler chicks with cardiomyopathy and ascites (17). It was also recently documented, by use of this immunoassay, that cTnT is found in high concentration in canine myocardium and is more easily measurable than CK-MB (18).

Although the cTnT immunoassay may be a candidate blood test for the reliable and universal discrimination between cardiac and muscle injury in veterinary clinical pathology, its tissue specificity has been recently questioned. Unexplained apparent increases in cardiac cTnT concentration have been associated with skeletal muscle injury or disease, multi-organ disease, and uremia (1). Recently it has been documented that the cardiac cTnT immunoassay detects activity in skeletal muscle, although at only a hundredth of the activity found in cardiac muscle (19).

The study reported here was undertaken to further evaluate cTnT as a biomarker of cardiac injury in laboratory animals. Specifically, we tested the hypotheses that serum cTnT: was applicable in laboratory animals (rats, dogs, mice, and ferrets) as a biomarker of cardiac injury arising from various causes (ischemia/reperfusion, doxorubicin administration, trauma, cardiac puncture); increased in proportion to the severity of cardiac injury; and was more cardiospecific and sensitive than CK or LD isozymes.

Materials and Methods

Animal models: Experimental procedures followed the guidelines of the *Guide for the Care and Use of Laboratory Animals* (National Institutes of Health) and were approved by the Institutional Animal Care and Use Committees. Blood samples used in this study were collected from animals being used for other investigative studies.

Purpose-bred, mixed-breed dogs (Butler Farms, Clyde, N.Y. [experiment 1] and Hazelton, Cumberland, Va. [experiment 2]) weighing 14 to 22 kg were used in two studies of myocardial ischemia/reperfusion (IR) injury after acclimation for at least 7 days. In the first experiment, we assessed the timing and amount of release of cTnT and CK-MB, compared with severity of cardiac injury. In a second experiment, dogs were allowed to recover after anesthesia and surgery, and we assessed cTnT, CK-MB, and LH-1 and LH-2 as indicators of cardiac injury in the presence of skeletal muscle injury associated with surgery and recovery from anesthesia.

To determine whether cTnT was a good indicator of cardiac injury in other species, we used a similar model of IR injury in the rat. To demonstrate that toxic injury could also be detected by cTnT, we induced doxorubicin cardiotoxicosis in mice. To determine whether route of collection affected cTnT, we used cardiac puncture under anesthesia in ferrets.

Ischemia/reperfusion injury in dogs. *Experiment 1:*

After an overnight nonfeeding period, nine dogs were anesthetized with dialurethane (approximately 0.6 ml/kg of body weight intravenously [i.v.]), intubated, and ventilated with 100% oxygen. Anesthesia depth; hemodynamic, electrocardiographic, blood gas, and serum electrolyte variables; and rectal temperature were monitored. Ringer's solution was administered i.v. at the rate of 3 ml/kg/h. Body temperature was maintained with a heating pad.

After left thoracotomy and insertion of a transducer-tipped catheter through a stab wound in the apex of the heart, a segment of the left cranial descending coronary artery (LCD) was dissected free of surrounding tissue, and a silk (1-0) ligature was placed under the LCD. Segment shortening in the region perfused by the LCD was assessed by use of a set of piezoelectric crystals inserted 4 to 6 mm into the myocardium.

After a stabilization period, the LCD was occluded for 90 min with a vascular clamp. Arterial blood samples were collected 1 min before and 60, 90, 150, 210, 270, and 360 min after occlusion into 0.1 volumes of 3.8% trisodium citrate and centrifuged at 1,000 X g for 10 min. Plasma was stored at -20°C until assayed for CK activity cTnT concentration.

Myocardial infarct size was then determined, using 2,3,5-triphenyl-tetrazolium chloride (TTC) and Evans blue stains (Sigma Chemical Co., St. Louis, Mo.). At the end of the experiment, Evans blue dye was injected into the right atrium while saline was perfused at a pressure of 100 mm Hg through a cannula placed into the LCD at the site of the original occlusion. The nonischemic area of the heart was stained blue; the area at risk remained unstained because of the infusion of saline. Dogs were then euthanized by administration of a barbiturate overdose, the heart was removed, and the left ventricle was serially sectioned from apex to base. The unstained and blue-stained areas were separated and incubated in phosphate buffer containing triphenyl-tetrazolium. Nonischemic myocardium stained red (due to the presence of dehydrogenase enzymes in viable tissue); ischemic myocardium remained unstained. Ischemic and nonischemic areas were separated and weighed. The weight of the ischemic area was used as an estimate of myocardial infarct size.

Experiment 2: For the second experiment on IR injury, five dogs were anesthetized and monitored as described previously. Myocardial ischemia was induced for 90 min, similar to conditions in experiment 1. Up to six electrodes were sutured into the heart for electrocardiographic studies. A permanent critical stenosis was also induced in the LCD, using suture and an 18- to 20-gauge needle, which was removed after suture placement. Incisions were closed, and the lungs were overinflated to evacuate pneumothorax through a tube, which was then removed. Blood samples were obtained 24 h after LCD occlusion and were compared with those obtained during the acclimation period.

Ischemia/reperfusion injury in rats: Five fed Sprague Dawley rats (Taconic Farms, Germantown, N.Y.) were anesthetized with urethane (1.25 g/kg, given intraperitoneally) and were ventilated with room air through a tracheotomy incision. Anesthesia depth, blood pressure, electrocardio-

graphic variables, and rectal temperature were monitored. Body temperature was maintained at 37°C with electric heating pads.

After left thoracotomy the heart was exposed, and a silk ligature (6-0), within a short length of polyethylene tubing, was placed around the LCD. The LCD was then occluded for 90 min by clamping the tubing against the heart surface, using 25-mm Schwartz forceps. At 45 min after initiation of ischemia, and 10, 70, 130, 190, and 270 min after occlusion, arterial blood samples were collected into serum separator tubes. Serum was stored at -20°C until assayed for CK activity and cTnT concentration.

At the end of the experiment, the portion of the left ventricle affected by LCD occlusion and at risk for ischemia was identified by the permanent re-occlusion of the LCD and the administration of a 10 mg/ml solution of Evans blue stain via the jugular cannula. The stained heart was rapidly excised, homogenized, and assayed for CK activity. Myocardial infarct size is known to be inversely correlated with myocardial CK activity (20, 21).

Doxorubicin-induced cardiotoxicosis in mice: Four male and four female mice (Charles River, Kingston, N.Y.), aged 7 weeks, were given 10 mg of doxorubicin/kg daily by single intraperitoneal injection. After 5 days of treatment mice were euthanized, and blood was collected from the abdominal aorta. This dosage of doxorubicin has been documented (22, 23) to induce marked degenerative cardiomyopathic changes. Three healthy mice were used as controls. Because of the low blood yield (50 to 250 µl), samples were pooled for each group. Serum was prepared and analyzed for cTnT concentration.

Cardiac puncture in ferrets: Seven male fitch ferrets (Triple F Farms, Sayre, Pa.) were anesthetized with ketamine for approximately 45 min, then approximately 1 ml of blood was collected by cardiac puncture immediately after induction of anesthesia and after 45 min of anesthesia. After blood collection, ferrets were euthanized by barbiturate overdose. Serum was prepared and analyzed for cTnT concentration.

Troponin T determination: Concentration of cTnT was determined, using the first commercially available (first-generation) enzyme-linked immunoassay (Elisa Troponin-T; Boehringer Mannheim Corp., Indianapolis, Ind.) (24), in all studies except the study in which serum cTnT concentration was determined in dogs 24 h after IR injury. For the latter, the currently marketed version (second-generation) of this immunoassay (Cardiac T Troponin T; Boehringer Mannheim Corp.) (25) was used. Compared with the first-generation assay, the second-generation assay has approximately 10-fold greater specificity for cardiac cTnT, but yields a similar standard curve (19, 24, 25). This difference has been attributed mainly to replacement of the polyclonal cTnT antibody (1B-10) used in the first-generation assay by a monoclonal antibody (M-7) in the second-generation assay (24, 25). Both assays use mouse monoclonal antibodies (M11-7) against human cTnT to label the captured cTnT. Both assays also use cTnT standards purified from bovine hearts.

All tests were done with an automated immunoanalyzer

(ES300AL; Boehringer Mannheim Corp.). Absorbance at 420 nm was determined and compared with that for standards supplied by the manufacturer (Boehringer Mannheim Corp.) and containing bovine cTnT (0, 1.2, 2.9, 5.5, 10.6, and 15.8 ng/ml for the first-generation assay and 0, 0.4, 1.2, 5.45, and 16.6 ng/ml for the second-generation assay). The measuring range was approximately 0 to 17 ng/ml, with 0.04 ng/ml being the lower detection limit. Analytical coefficients of variation were <3%.

In addition to the aforementioned determinations, mean values for serum cTnT and isozymes of CK and LD were obtained from 10 healthy and untreated dogs of mixed breed and the same size as the experimental dogs, and 12 healthy, untreated Sprague Dawley rats.

Extended cTnT standard curve: For most serum samples, concentrations of cTnT were determined by the automated analyzer using standards provided by the manufacturer the assay kits. However, for several samples, absorbance was outside the range of these standards, and there was insufficient sample volume to dilute them and repeat the analysis. To extend the standard curve for determination of the cTnT concentration of these samples, diluted homogenates of myocardium were included as additional standards.

Before using these myocardial specimens as additional standards, their cTnT concentration was first determined. Because our studies indicated that myocardial cTnT concentration was similar among mammals, we used myocardium from different species (two rats, two pigs, one goat) that were conveniently available. Approximately 500 mg of myocardium was placed in four volumes (approximately 2 ml) of 1M KCl, 10 mM imidazole, and 0.5 mM dithiothreitol, then was homogenized on ice for three intervals of 10 sec separated by 30-sec rest periods, using a tissue homogenizer (Tissumizer; Tekmar Co., Cincinnati, Ohio) set at full speed. Homogenates were diluted 100,000-fold (volume of diluted homogenate/weight of myocardium used for homogenization) with cTnT-free human serum (Diluent Troponin-T; Boehringer Mannheim Corp.), and their cTnT concentration was determined from the absorbance and the curve for standards supplied by the manufacturer.

Four standards of known cTnT concentration were prepared by specific serial dilutions (1,000-, 10,000-, 100,000-, and 100,000-fold) of the myocardium for which the cTnT concentration was determined. Using the standards supplied by the manufacturer and those that we had prepared, the extended standard curve was then generated from the known cTnT concentrations and their measured absorbances. To prevent any cross-contamination due to carry-over, each series of diluted homogenates was assayed, starting with the most diluted and progressing to the most concentrated. Furthermore, each of the five tissue specimens was analyzed on a separate day and after thorough cleaning of the sampling pipette of the immunoanalyzer.

Determination of LD and CK activities: Total CK activity for experiment 2 of the canine studies and total LD activity were determined at 37°C, using an automated chemistry analyzer and the accompanying reagent system

(Hitachi 717 Automated Chemistry Analyzer; Boehringer Mannheim Corp.). Total CK activity for the remainder of the studies was determined at 37°C by a manual procedure, using a commercially available assay kit (Sigma Chemical Co.). For estimation of the severity of infarction in rats, myocardial specimens were homogenized in 4 ml of 250 mM sucrose, 1 mM EDTA, and 10 mM β -mercaptoethanol prior to analysis. Both CK assays use a coupled enzyme method based on that of Oliver (26) and Rosalki (27). Total LD activity was estimated from the increase in absorbance at 340 nm resulting from the conversion of lactate to pyruvate and reduction of NAD⁺ to NADH (28).

Isozymes of CK and LD were separated, using agarose gel electrophoresis (75 μ l, 0 mA, 1,000 V, 10°C, 5 min for LD; 75 μ l, 0 mA, 1,200 V, 13°C, and 2.3 min for CK) and an automated analyzer (Helena Rapid Electrophoresis Analyzer and Electrophoresis Data Center; Helena Laboratories, Beaumont, Tex.) with the accompanying reagent system (REP LD-30 and REP CK-MM6 Isoenzyme Procedures; Helena Laboratories). Activities were visualized, using enzymatic reactions similar to those used to determine total CK and LD activities, at 45°C for 10 and 4.5 min, respectively, then were measured by fluorescence densitometry. Absolute isozyme activities were calculated from the total enzyme activity and the proportion of total staining attributable to each isozyme.

Statistical analysis: Statistical computations and figures were made with commercially available software (Graphpad Prism and InStat; Institute for Scientific Information, Philadelphia, Pa.). Values are reported as mean \pm SEM. Mean cardiac cTnT concentrations for the various groups were compared by use of the Student's *t* test (nonpaired, two-sided), except when variances differed between groups, in which case Welch's alternate *t* test was used. When distribution of values was considered nonGaussian and skewed because they were near zero and outside the accurately measurable range, such as the pre-IR values for cTnT and postischemia values for CK-MB and CK-BB, groups were compared by the Mann-Whitney (nonpaired, two-sided, nonparametric) test. Linear regression analysis was performed by use of the least squares method to test for correlation between parameters. Nonlinear regression analysis, using a hyperbolic curve, was performed to define the relationship between cTnT concentration and absorbance for the extended standard curve, and between biomarker concentrations and time of reperfusion. Differences in biomarker concentrations over time were also compared by one-way analysis of variance (ANOVA), and when the *F* statistic indicated between-group differences, by a Student-Newman-Keuls post-hoc analysis. When the variances of means compared by ANOVA were unequal according to Bartlett's test, data were logarithmically transformed before analysis. Differences were considered statistically significant at $P < 0.05$.

Results

Extended cTnT standard curve: Absorbance from 0 to approximately 3 was linearly related to cTnT concentra-

tion between 0 and approximately 15 ng/ml ($R^2 = 0.99$; $P < 0.0001$). The cTnT concentration for all but six serum samples, for which there was insufficient volume to dilute, was determined within this absorbance range: three dog serum samples yielded absorbances of 3.02, 3.23, and 3.89, and three ferret samples yielded absorbances of 5.43, 6.11, and 7.82. Using this linear relationship and concentration range and the first-generation assay, mean SEM cTnT concentration in myocardium of mammals (two rat, two pig, one goat) was determined from 100,000-fold diluted homogenates to be 465 ± 20 mg/g wet weight. Using mammalian myocardium as a source of standards with high cTnT concentration, the standard curve was extended to 500 ng/ml. The relationship between absorbance and concentration was shown to be hyperbolic ($R^2 = 1.00$), with maximal absorbance of 9.7 and half-maximal absorbance at 32.6 ng of cTnT/ml.

Ischemia/reperfusion in the dog: Compared with healthy, unoperated dogs, serum cTnT concentration was significantly increased by the anesthetic, surgical, and instrumentation procedures used in preparation of dogs for occlusion of the LCD: 0.62 ± 0.13 ng/ml at 1 min prior to occlusion versus 0.01 ± 0.00 ng/ml. However, 60 and 90 min of ischemia did not induce any further increase in serum cTnT values: 0.44 ± 0.10 and 0.42 ± 0.09 ng/ml, respectively.

Because tissue injury and increases in serum biomarkers were minimal, values for one dog were excluded from the analysis of the time course of postinfarction increase in serum biomarkers. Compared with values for the other eight dogs, the myocardial infarct in this dog was 0.31 g (versus 2.00 to 18.72 g), and after 4.5 h of reperfusion, serum cTnT concentration was only 0.28 ng/ml (versus >2 ng/ml) and serum total CK activity was only 360 U/L (versus 600 to 3,500 U/L).

There was a significant trend for serum cTnT concentration to increase with time of reperfusion. Compared with serum cTnT values at the beginning of reperfusion in the eight dogs with appreciable infarcts, there was a 10- to 30-fold increase in serum cTnT concentration at all time points studied after reperfusion. During the first 3 h, cTnT values increased at a rate of approximately 3 ng/ml/h, and continued to increase by 1.5 ng/ml in the fourth h of reperfusion (Figure 1). Data fit a hyperbola ($R^2 = 1.00$) indicating that serum cTnT concentration would be maximal at 53 ng/ml and would be half-maximal at 12 h.

There was a significant trend for serum total CK activity to increase with time of reperfusion. Compared with serum total CK values at the beginning of reperfusion in the eight dogs with appreciable infarcts, there was a 3- to 9-fold increase in serum total CK activity at all time points after reperfusion. During the first 3 h, serum CK activity increased in similar manner as did cTnT concentration, but with less regularity and lesser amount. Serum CK activity increased 2- to 4-fold, by 400 to 900 U/L/h for the first 3 h, then remained constant during the fourth h. Data fit a hyperbola ($R^2 = 1.00$) indicating that serum total CK activity would be maximal at 3,600 U/L, and was half-maximal at 2.5 h.

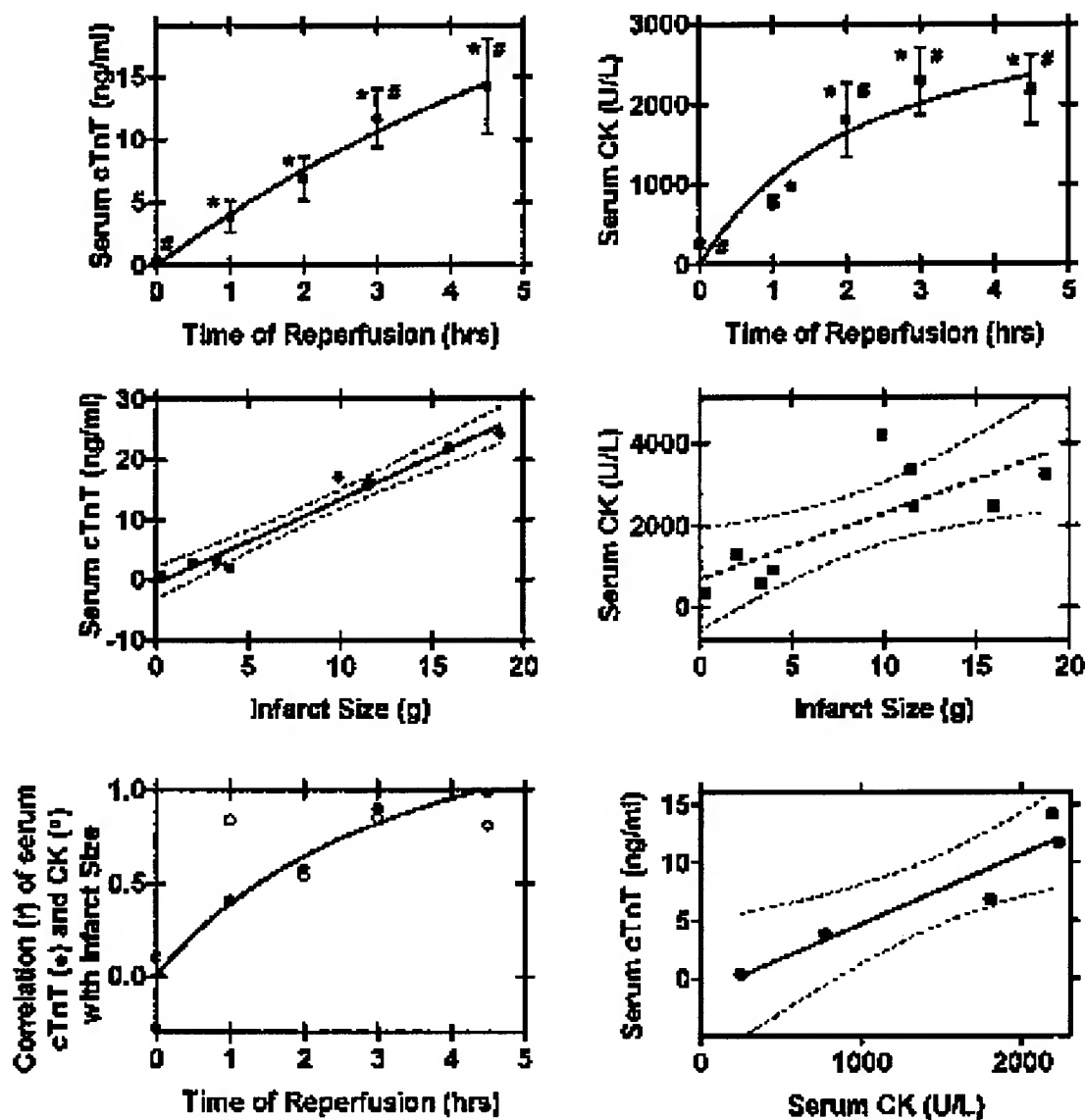


Figure 1. Relationships of serum values of cardiac troponin T (cTnT) and creatine kinase (CK) to the timing and severity of myocardial infarction in dogs. Mean (\pm SEM) values were determined during the first 4.5 h of reperfusion after coronary artery occlusion. In the upper graphs, serum values of cTnT and CK are plotted against duration of reperfusion. Values different from those at the beginning of reperfusion (*), and after 1 h of reperfusion (#), are indicated. In the middle graphs, maximal serum cTnT concentration and CK activity are plotted against infarct size; the linear regression line and its 95% confidence interval are shown. In the left lower graph, plots of the correlation (coefficient, r) of serum cTnT concentration and CK activity with infarct size against duration of reperfusion are shown to fit a hyperbolic curve. In the right lower graph, serum cTnT concentration is plotted against serum CK activity; the linear regression line and its 95% confidence interval are shown.

The infarct size was highly correlated with the maximal increase in serum CK activity ($r = 0.78$; $P < 0.01$) and especially for cTnT concentration ($r = 0.98$; $P < 0.0001$); 96 and 60% of the variation in serum cTnT and CK, respectively, could be attributed to infarct size (Figure 1). The degree of correlation of serum cTnT with infarct size progressively and hyperbolically increased over time of reperfusion, exceeding 0.9 by 3 h and peaking at approximately 4.5 h.

Correlation of serum CK activity with infarct size was less regular, but also increased over time. Serum cTnT concentration and CK activity were highly correlated ($r = 0.95$; $P = 0.01$) during reperfusion, with 6.0 ± 1.2 ng of cTnT released per U of CK.

In the second experiment, in which dogs were subjected to IR then allowed to recover for 24 h, the effects of IR on serum enzyme activities were variable. Individual values

Table 1. Serum lactate dehydrogenase (LD), creatine kinase (CK), and cardiac troponin T (cTnT) values before and after myocardial injury induced by ischemia/reperfusion (IR)

Serum biomarker	Dog 1	Dog 2	Dog 3	Dog 4	Dog 5	Mean	SEM
LD-1							
Pre-IR (U/L)	40.1	19.9	19.8	27.0	14.7	24.3	4.4
(%)	17.9	28.0	27.8	14.4	27.2	23.1	2.9
Post-IR (U/L)	22.1	139.3	61.5	28.2	99.2	70.1	22.1
(%)	17.2	51.0	34.9	22.4	38.9	32.9	6.0
LD-2							
Pre-IR (U/L)	17.3	13.7	11.4	12.4	0.6	11.1	2.8
(%)	7.7	19.3	16.0	6.6	1.2	10.2	3.3
Post-IR (U/L)	22.5	68.7	42.8	23.6	66.7	44.9	10.0*
(%)	17.5	25.2	24.3	18.7	26.2	22.4	1.8*
LD-(1 + 2)							
Pre-IR (U/L)	57.4	33.6	31.2	39.4	15.3	35.4	6.8
(%)	25.6	47.3	43.8	21.0	28.4	33.2	5.2
Post-IR (U/L)	44.6	208.0	104.3	51.8	165.9	114.9	31.9*
(%)	34.7	76.2	59.2	41.1	65.1	55.3	7.7*
LD-3							
Pre-IR (U/L)	29.1	14.8	8.4	24.9	5.8	16.6	4.5
(%)	13.0	20.8	11.9	13.3	10.7	13.9	1.8
Post-IR (U/L)	25.7	27.9	37.3	25.1	34.3	30.1	2.4*
(%)	20.1	10.2	21.2	19.9	13.4	17.0	2.2
LD-4							
Pre-IR (U/L)	35.7	7.2	7.0	33.5	17.0	20.1	6.2
(%)	15.9	10.1	9.8	17.8	31.4	17.0	2.2
Post-IR (U/L)	18.2	10.3	13.2	15.7	18.1	15.1	1.5
(%)	14.2	3.8	7.5	12.5	7.1	9.0	1.9
LD-5							
Pre-IR (U/L)	101.7	15.4	24.5	90.1	16.0	49.5	19.1
(%)	45.4	21.7	34.5	47.9	29.6	35.8	4.9
Post-IR (U/L)	39.6	26.7	21.2	33.3	36.7	31.5	3.4
(%)	31.0	9.8	12.0	26.4	14.4	18.7	4.2*
LD-Total							
Pre-IR (U/L)	224.0	71.0	71.0	188.0	54.0	121.6	35.1
Post-IR (U/L)	128.0	273.0	176.0	126.0	255.0	191.6	31.0
CK-MM							
Pre-IR (U/L)	122.0	145.0	125.0	154.0	33.5	115.9	21.5
(%)	62.6	81.9	76.0	67.2	35.6	64.7	8.0
Post-IR (U/L)	5,230.0	7,606.0	5,866.0	1,384.0	9,570.0	8,422.0	1,550.0*
(%)	100.0	98.0	97.3	100.0	100.0	99.1	0.6*
CK-MB							
Pre-IR (U/L)	5.1	7.9	11.7	5.2	8.2	7.6	1.2
(%)	2.6	4.4	7.1	2.3	8.7	5.0	1.3
Post-IR (U/L)	0	154.0	164.0	0	0	63.6	39.0
(%)	0	2.0	2.7	0	0	0.9	0.6*
CK-BB							
Pre-IR (U/L)	67.9	24.2	27.9	69.8	52.3	48.4	9.6
(%)	34.8	13.7	16.9	30.5	55.7	30.3	7.5
Post-IR (U/L)	0	0	0	0	0	0	0*
(%)	0	0	0	0	0	0	0*
CK-Total							
Pre-IR (U/L)	195.0	177.0	165.0	229.0	94.0	172.0	22.3
Post-IR (U/L)	5,230.0	7,760.0	6,030.0	1,384.0	9,570.0	8,486.0	1,533.0*
cTnT							
Pre-IR (ng/ml)	0.024	0	0	0.009	0.016	0.010	0.005
Post-IR (ng/ml)	2.62	14.81	3.003	0.406	27.41	9.65	5.10*

*Significantly different from corresponding pre-IR value.

are, therefore, reported for each dog in addition to mean values for all dogs (Table 1). Compared with pre-IR values, recovered dogs had 1,000-fold increased serum cTnT concentration, and 49-fold increased serum total CK activity, but no detectable change in serum total LD activity. The increased total CK activity was attributable to increased CK-MM isozyme activity, which was so large that it prevented detection of CK-MB and CK-BB activities. In contrast to total CK, total LD activity was not increased in recovered dogs, although absolute and relative activities of the cardiac LD isozymes were increased approximately 3- and 2-fold, respectively. These latter increases caused a

decrease in the relative activity of skeletal muscle LD isozyme, the absolute activity of which was not changed after IR and recovery.

Serum cTnT concentration in the dogs recovered from the IR treatment was highly correlated ($R^2 = 0.96$; $P = 0.004$) with the activity of cardiac isozymes of LD (LD-1 and LD-2), but was unrelated to activity of the skeletal muscle isozymes of CK (CK-MM; $R^2 = 0.00$; $P = 0.96$) and LD (LD-5, which remained constant).

In the rats subjected to IR, the increases in serum cTnT concentration were variable, similar to values in dogs of the second IR experiment. Individual values are, therefore,

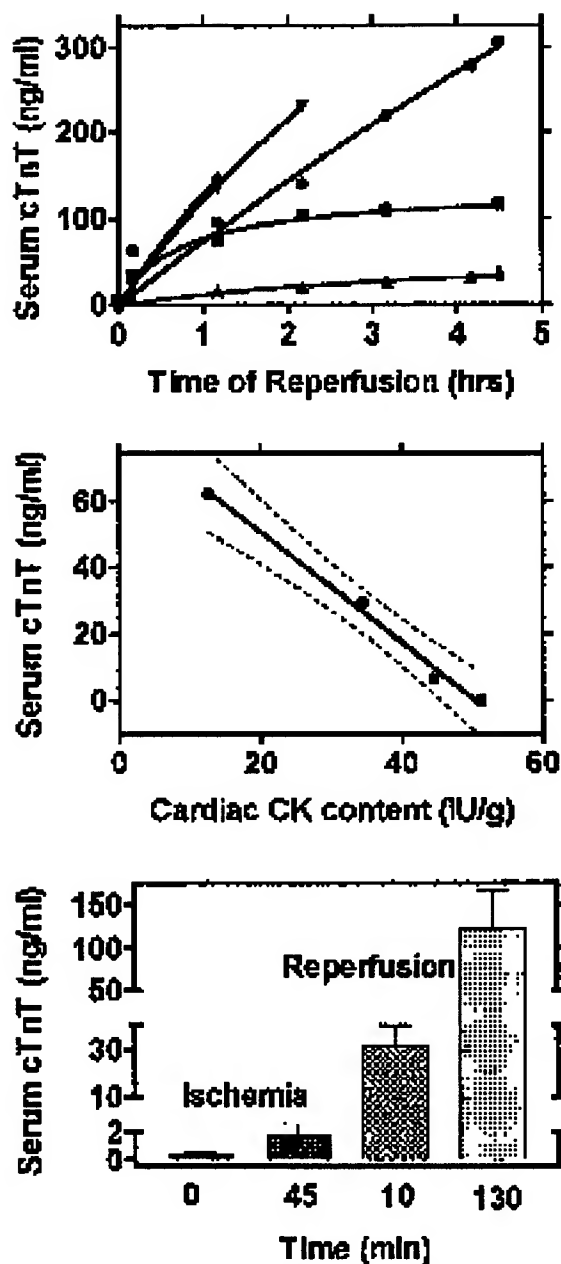


Figure 2. Relationship of serum values of cTnT to the timing and severity of myocardial infarction in rats. Activities were determined during the first 4.5 h of reperfusion after coronary artery occlusion. In the upper graph, serum cTnT concentration is plotted against duration of reperfusion for each of five rats. In the middle graph, serum cTnT concentration is plotted against severity of injury, as indicated by the myocardial content of CK; the linear regression line and its 95% confidence interval are shown. In the lower graph, mean (\pm SEM) serum cTnT concentration is shown for rats prior to ischemia, after 45 min of ischemia, and after 10 and 130 min of postischemia reperfusion.

reported for each rat in addition to mean values for all rats (Figure 2). Serum cTnT concentration was 0.01 ± 0.00 ng/ml in 12 untreated rats, 50-fold higher after preparing the rats for clamping of the LCD, 200-fold by 45 min of ischemia, 3,000-fold after 10 min of reperfusion, and 10,000-fold by 130 min of reperfusion (Figure 2). In each instance, the data describing the time course of the increase in serum cTnT concentration during the observed postreperfusion time fit a hyperbola ($R^2 = 0.96$ to 1.00). As an indicator of severity of infarction, myocardial total CK activity was determined in nine rats not subjected to IR (51.3 ± 1.7 U/g wet weight) and in three of the five rats subjected to IR. These activities were highly and inversely correlated with serum cTnT concentration ($R^2 = 0.99$; $P = 0.004$; Figure 2).

In 10 healthy mice, serum cTnT concentration was 0.19 ± 0.027 ng/ml, approximately 20-fold higher than that found in other species (rats, dogs, ferrets, humans). Serum cTnT concentration of pooled blood from male and female mice treated with doxorubicin was increased 10-fold, compared with the value in controls (Figure 3).

In the ferrets from which blood was collected by cardiac puncture on two separate intervals separated by 45 min, the serum cTnT concentration was highly variable, ranging from 0.1 to 133 ng/ml (Figure 3). Because cTnT was undetectable in untreated healthy ferrets (unpublished data), these values indicate marked increase in serum cTnT concentration in association with cardiac puncture. There was no difference in serum cTnT concentrations measured at different time points after induction of anesthesia.

Discussion

In this study, several novel findings confirmed and extended reported results (12–17), indicating that the occurrence and severity of cardiac injury in various laboratory animals can be reliably determined from serum cTnT concentration. The serum cTnT assay is shown to be effective at detecting cardiac injury induced by various causes, including ischemia, IR, doxorubicin, and physical injury, in various laboratory animal species, including rats, mice, dogs, and ferrets. Importantly and uniquely, results of this study clearly indicate that, in the presence of moderate skeletal muscle injury, serum cTnT is an effective indicator of cardiac injury, whereas cardiac isozymes of LD, and especially of CK, are ineffective biomarkers of cardiac injury. Furthermore, within 3 h of cardiac injury, serum cTnT concentration is an accurate predictor of severity of the injury, and more accurately predictive of cardiac origin than is CK, even in the absence of skeletal muscle injury. Serum cTnT concentration after IR was more than 1,000-fold greater than control values, whereas total CK activity of cardiac origin and cardiac LD and CK isozyme activities were typically <10-fold greater than controls.

Our finding that serum cTnT concentration is proportional to infarct size in rats and dogs is supported by results of previous studies. A study of four dogs indicated that, within 3 weeks of LCD occlusion, maximal serum concentration of cTnT, but not activity of cardiac CK isozymes, correlated with infarct size (16). Results of studies of isolated and perfused rat hearts (13, 29–33) indicated that

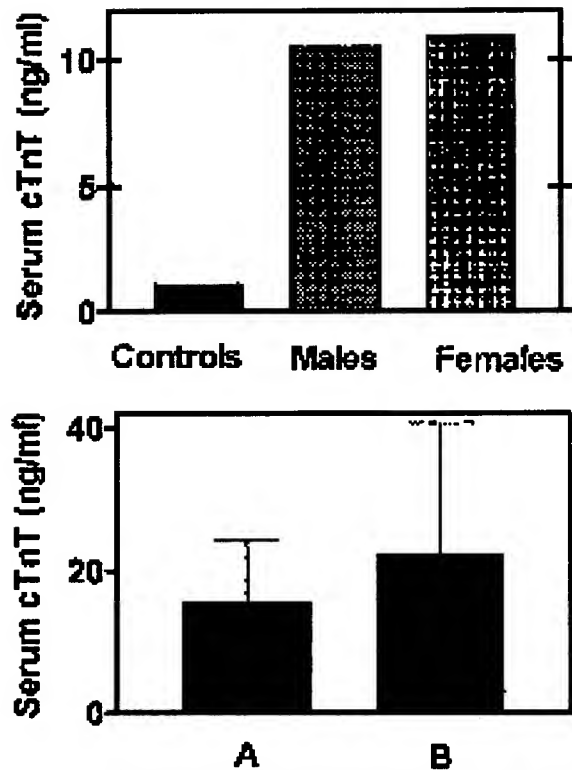


Figure 3. Serum values of cTnT in mice with doxorubicin-induced cardiotoxicosis and in ferrets that underwent cardiac puncture. In the upper bar graph, serum cTnT concentration is shown for pooled blood samples from three control mice and four male and four female mice treated for 5 days with doxorubicin. In the lower bar graph, serum cTnT concentration is shown for blood collected by cardiac puncture from ferrets under anesthesia, at the beginning of anesthesia (A) and after 45 min of anesthesia (B).

cTnT concentration was correlated with duration of ischemia and with hemodynamic dysfunction. In rats receiving abdominal, heterotopic heart transplants (14) and in rats administered cardiotoxic doses of isoprenaline (12), serum cTnT concentration correlated with severity of histologic indication of degeneration.

Comparison of cTnT, CK, and LD as biomarkers of cardiac injury: Our experiments in dogs indicated that cTnT, but not CK-MB or LDH-1, is an effective marker of cardiac injury with coexisting moderate (serum CK of 5,000 to 14,000 U/L) muscle injury. Enzymes were released from myocardium during IR and from skeletal muscle after the dogs were revived. Cardiac origin of increased serum CK activity during IR was indicated by its high correlation with serum cTnT concentration and infarct size; muscle origin of increased serum CK activity in revived dogs was indicated by lack of these correlations. Furthermore, isozyme analysis for revived dogs indicated that LD release, which follows CK release, had occurred from myocardium but had not yet occurred from skeletal muscle. Muscle injury was likely caused by ischemia secondary to LCD occlusion and

stenosis. Associated enzyme increases were likely delayed until resumption of muscular activity.

Even in the absence of moderate skeletal muscle injury, which caused CK to be of little diagnostic value for myocardial infarct, serum cTnT concentration was superior to serum activities of CK isozymes as a biomarker of cardiac injury. Compared with CK values, cTnT concentration in serum had higher correlation ($r = 0.96$ versus 0.60) with severity of myocardial injury, was not found in appreciable amounts in control samples, and consequently, was increased, relative to control values, by more than a 100-fold. Furthermore, in a previous study (16) of cTnT and CK after LCD occlusion, infarct size was more highly correlated with cTnT concentration ($r = 0.93$ versus 0.56). Finally, in addition to the cTnT assay being more effective in detection of cardiac injury than are assays of CK and LD isozyme activities, we found it to be more easily and rapidly performed and therefore less expensive per assay (data not presented).

Our finding that cTnT is a more sensitive marker than CK-MB is confirmed by a study of cardiac rejection in rats (14). In this study, cTnT was increased 10-fold with earliest histologic signs (edema) of rejection, whereas CK-MB values were not significantly different from control values. Furthermore, serum cTnT concentration was significantly correlated with severity of rejection.

Serum cTnT concentration in various species and various cardiac injuries: Serum cTnT concentration was also shown to be an effective indicator of the occurrence and severity of myocardial infarction in rats. Furthermore, using the rat model, it was shown that prior to reperfusion, ischemia alone caused increases in serum cTnT concentration. The effect of ischemia, prior to reperfusion, on serum cTnT concentration was not observed in dogs, possibly because it was masked by the release of cTnT associated with incision into the myocardium for catheter insertion, which induced a 50-fold increase in cTnT values. Manipulation of the rat heart prior to occlusion of the LCD apparently induced a similar increase in serum cTnT concentration.

Our *in vivo* studies of cTnT during IR in rats confirm and extend previous studies that were conducted using isolated and perfused rat hearts (13, 29–33). Here we quantify the increase in serum cTnT concentration associated with myocardial infarction in rats and indicate correlation of cTnT concentration with severity of injury.

Our studies of doxorubicin cardiotoxicosis in mice indicate that degenerative effects induced chemically also result in marked increases in serum cTnT concentration. The association of increased serum cTnT concentration with degenerative cardiotoxicosis was also found in rats administered isoprenaline (12).

Blood sample collection by cardiac puncture, although a relatively common and accepted method used terminally in laboratory animals (28), is clearly documented in this study to be inappropriate for evaluation of cardiac injury. A similar conclusion was made from studies of mice (15). Increases in serum cTnT concentration (Figure 3) induced by use of this blood collection method were highly variable, ranging from slight to marked. This variation, and

the fact that a second cardiac puncture did not further increase serum cTnT values, probably result from the fact that most of the cTnT increase was attributable to direct tissue contamination rather than to release of cTnT into blood.

Qualifications, limitations, and needs for further studies: In interpretation of the results of this study, its limitations should be considered. The number of animals used was small. However, results had high significance because cTnT is a highly effective indicator of cardiac injury, differences from controls were large, and correlations between parameters were high. Only selected species were studied, including dogs, mice, rats, and ferrets. However, these are the laboratory animals commonly used in research, and previous studies have indicated that cTnT reactivity and specificity are conserved across a wide range of species. It is noteworthy that of these species, mice had substantially higher baseline values than those found in other species. This may reflect the fact that the monoclonal antibodies used in the immunoassay were produced using hybridomas of mouse origin (24). This conclusion is supported by the observation that isolated mouse cTnT is 10-fold more reactive with monoclonal antibody M7, which is used in the cTnT immunoassay, than is isolated human cTnT (15).

In most of our studies, we used the first-generation cTnT immunoassay (24), which is now being replaced by a second-generation cTnT immunoassay (25). In a comparative study of these two assays, it was documented that the second-generation assay differed from the first-generation assay principally in having 10-fold improved cardiospecificity (19). It was 100-fold more reactive with cardiac than with skeletal muscle, whereas for the first-generation assay, there was only a 10-fold difference in tissue reactivities. Because the second-generation assay was substantially improved over the first-generation assay, this difference should only reinforce our conclusion that cTnT is a highly effective biomarker of cardiac injury. Furthermore, in this study, we used the second-generation assay in evaluation of cTnT cardiospecificity in the presence of skeletal muscle injury.

Measurements of enzyme mass are more sensitive than are measurements of enzyme activity, which is more labile (1). Thus, measurement of CK-MB mass should have increased effectiveness in detection and assessment of cardiac injury. However, diagnostic use of either CK-MB activity or mass is limited by high baseline CK-MB activity in some species and by co-existing skeletal muscle injury. Furthermore, species-specific immunoassays for CK-MB are not commercially available for use in laboratory animals, and CK-MB immunoreactivity is not well conserved across species (unpublished data).

Although cTnT is effective for evaluation of acute or ongoing cardiac injury in the presence of mild to moderate injury of skeletal muscle, further studies are required to define the severity of skeletal muscle injury that interferes with the cTnT assay effectiveness. Also, further studies of the kinetics of release and clearance of cTnT in different species are required to define the duration of time from

injury in which cTnT is a useful biomarker.

We conclude that cTnT is a powerful biomarker in laboratory animals for the sensitive and specific detection of cardiac injury arising from various causes. The cTnT immunoassay is apparently the first commercially available assay documented to be universally applicable for this purpose. However, until the cTnT immunoassay's reactivity for skeletal muscle is further diminished in a third-generation assay, and until the species-dependence of the kinetics of cTnT release and clearance is defined, its use should be restricted to acute or ongoing cardiac injury, and results should be interpreted cautiously in the presence of moderate to marked skeletal muscle injury.

Acknowledgements

The authors thank Tracy Stewart (Human Safety Department, The Procter and Gamble Company) for her technical assistance. The Boehringer Mannheim Corporation donated troponin-T assay kits used in this study.

References

1. Keffer, J. H. 1996. Myocardial markers of injury. Evolution and insights. *Clin. Chem.* **105**:305-320.
2. Burger, A., R. Richterich, and H. Aepli. 1964. The heterogeneity of creatine kinase. *Biochem. Zeit.* **339**:305-314.
3. Thorén-Tolling, K., and L. Jönsson. 1983. Creatine kinase isoenzymes in serum of pigs having myocardial and skeletal muscle necrosis. *Can. J. Comp. Med.* **47**:207-216.
4. Cardinet, G. H. 1989. Skeletal muscle function, p. 462-495. In J. J. Kaneko (ed.), *Clinical biochemistry of domestic animals*. Academic Press, Inc., San Diego, Calif.
5. Alleyassine, H., and D. B. Tonks. 1978. Albumin-bound fluorescence: a potential source of error in fluorometric assay of creatine kinase BB isoenzyme. *Clin. Chem.* **24**:1849-1850.
6. Boyd, J. W. 1988. Serum enzymes in the diagnosis of disease in man and animals. *J. Comp. Pathol.* **98**:381-404.
7. Apple, F. S., and P. A. Tesch. 1989. CK and LD isozymes in human single muscle fibers in trained athletes. *J. Appl. Physiol.* **66**:2717-2720.
8. Yasuda, J., K. Tateyama, B. Syuto, *et al.* Lactate dehydrogenase and creatine phosphokinase isoenzymes in tissues of laboratory animals. *Jpn. J. Vet. Res.* **38**:19-29.
9. Friedel, R., and H. Mattenheimer. 1970. Release of metabolic enzymes from platelets during blood clotting of man, dog, rabbit and rat. *Clin. Chim. Acta* **30**:37-46.
10. Bhayana, V., and A. R. Henderson. 1995. Biochemical markers of myocardial damage. *Clin. Biochem.* **28**:1-29.
11. Malouf, N. N., D. McMahon, A. E. Oakeley, *et al.* 1992. A cardiac troponin T epitope conserved across phyla. *J. Biol. Chem.* **267**:9269-9274.
12. Bleuel, H., U. Deschl, T. Bertsch, *et al.* Diagnostic efficacy of troponin T measurements in rats with experimental myocardial cell damage. *Exp. Toxic. Pathol.* **47**:121-127.
13. Remppis, A., T. Scheffold, J. Greten, *et al.* 1995. Intracellular compartmentation of troponin T: release kinetics after global ischemia and calcium paradox in the isolated perfused rat heart. *J. Mol. Cell. Cardiol.* **27**:793-803.
14. Walpoth, B. H., A. Tschopp, E. Peheim, *et al.* 1995. Assessment of troponin-T for detection of cardiac rejection in a rat model. *Transplantation Proc.* **27**:2084-2087.
15. Bachmaier, K., J. Mair, F. Offner, *et al.* 1995. Serum cardiac troponin T and creatine kinase-MB elevations in murine autoimmune myocarditis. *Circulation* **92**:1927-1932.

16. Voss, E. M., S. W. Sharkey, A. E. Gernert, *et al.* 1995. Human and canine cardiac troponin T and creatine kinase-MB distribution in normal and diseased myocardium. Infarct sizing using serum profiles. *Arch Pathol. Lab. Med.* **119**:799-806.
17. Maxwell, M. H., G. W. Robertson, and D. Moseley. 1994. Potential role of serum troponin T in cardiomyocyte injury in the broiler ascites syndrome. *Br. Poult. Sci.* **35**:663-667.
18. O'Brien, P. J. 1997. Deficiencies of myocardial troponin-T and creatine kinase MB isozyme in dogs with idiopathic dilated cardiomyopathy. *Am. J. Vet. Res.* **58**:11-16.
19. O'Brien, P. J., G. W. Dameron, M. L. Beck, *et al.* 1996. Specificity in different species and in cardiac versus skeletal muscle of two generations of cardiac troponin-T immunoassays. Submitted for publication.
20. Griswold, D. E., D. E. Hillegass, D. E. Hill, *et al.* 1988. Method for quantification of myocardial infarction and inflammatory cell infiltration in rat cardiac tissue. *J. Pharmacol. Methods* **20**:225-235.
21. Murohara, T., J. P. Guo, J. A. Delyani, *et al.* 1995. Cardioprotective effects of selective inhibition of the two complement activation pathways in myocardial ischemia and reperfusion injury. *Methods Find. Exp. Clin. Pharmacol.* **17**:499-507.
22. Solcia, E., L. Ballerini, O. Bellini, *et al.* 1981. Cardiomyopathy of doxorubicin in experimental animals. Factors affecting the severity, distribution and evolution of myocardial lesions. *Tumori* **67**:461-472.
23. Schmitt-Graff, A., and M. E. Scheulen. 1986. Prevention of adriamycin cardiotoxicity by niacin, isocitrate or *N*-acetylcysteine in mice. A morphological study. *Path. Res. Pract.* **181**:168-174.
24. Katus, H. A., S. Looser, K. Hallermayer, *et al.* 1992. Development and in vitro characterization of a new immunoassay of cardiac troponin T. *Clin. Chem.* **38**:386-393.
25. Muller-Bardorff, M., K. Hallermayer, A. Schroder, *et al.* 1997. Improved troponin T ELISA specific for cardiac troponin T isoform: assay development and analytical and clinical validation. *Clin. Chem.* **43**:458-466.
26. Oliver, I. T. 1995. A spectrophotometric method for the determination of creatine phosphokinase myokinase. *Biochem. J.* **61**:116.
27. Rosalki, S. B. 1967. An improved procedure for serum creatine phosphokinase determination. *J. Lab. Clin. Med.* **69**:696-705.
28. Wacker, W. E. C., D. D. Ulmer, and B. L. Vallee. 1956. Metalloenzymes and myocardial infarction. *N. Engl. J. Med.* **255**:449-505.
29. Asayama, J., Y. Yamahara, B. Ohta, *et al.* 1992. Release kinetics of cardiac troponin-T in coronary effluent from isolated rat hearts during hypoxia and reoxygenation. *Basic Res. Cardiol.* **87**:428-436.
30. Asayama, J., Y. Yamahara, H. Miyazaki, *et al.* 1994. Effects of release kinetics of troponin T, creatine kinase, and lactate dehydrogenase in coronary effluent from isolated rat hearts. *Int. J. Cardiol.* **44**:131-135.
31. Saitoh, Y., K. Gu, S. Kin, *et al.* 1995. Ischemic preconditioning improves cardiac functional recovery following preservation with University of Wisconsin solution. *Transplantation* **60**:1079-1083.
32. Yamahara, Y., J. Asayama, B. Ohta, *et al.* 1993. Release kinetics and correlation with hemodynamic dysfunction of cardiac troponin-T in coronary effluent from isolated rat hearts during reperfusion. *Basic Res. Cardiol.* **88**:307-313.
33. Yamahara, Y., J. Asayama, J. Kobara, *et al.* 1994. Effects of ischemic preconditioning on the release of cardiac troponin T in isolated hearts. *Basic Res. Cardiol.* **89**:241-249.

Exhibit B

References Cited in Dr. Koshimizu's Declaration

M. Jain et al.

**“Cell Therapy Attenuates Deleterious Ventricular
Remodeling and Improves Cardiac Performance
After Myocardial Infarction”**

Circulation

JOURNAL OF THE AMERICAN HEART ASSOCIATION



Cell Therapy Attenuates Deleterious Ventricular Remodeling and Improves Cardiac Performance After Myocardial Infarction

Mohit Jain, Harout DerSimonian, Daniel A. Brenner, Soeun Ngoy, Paige Teller, Albert S. B. Edge, Agatha Zawadzka, Kristie Wetzell, Douglas B. Sawyer, Wilson S. Colucci, Carl S. Apstein and Ronglih Liao

Circulation 2001;103:1920-1927

Circulation is published by the American Heart Association, 7272 Greenville Avenue, Dallas, TX 75214
Copyright © 2001 American Heart Association. All rights reserved. Print ISSN: 0009-7322. Online ISSN: 1524-4539

The online version of this article, along with updated information and services, is located on the World Wide Web at:
<http://circ.ahajournals.org/cgi/content/full/103/14/1920>

Subscriptions: Information about subscribing to *Circulation* is online at
<http://circ.ahajournals.org/subscriptions/>

Permissions: Permissions & Rights Desk, Lippincott Williams & Wilkins, a division of Wolters Kluwer Health, 351 West Camden Street, Baltimore, MD 21202-2436. Phone: 410-528-4050. Fax: 410-528-8550.

E-mail:
journalpermissions@lww.com

Reprints: Information about reprints can be found online at
<http://www.lww.com/reprints>

Cell Therapy Attenuates Deleterious Ventricular Remodeling and Improves Cardiac Performance After Myocardial Infarction

Mohit Jain*; Harout DerSimonian, PhD*; Daniel A. Brenner, MA; Soeun Ngoy; Paige Teller, MA; Albert S.B. Edge, PhD; Agatha Zawadzka; Kristie Wetzel; Douglas B. Sawyer, MD, PhD; Wilson S. Colucci, MD; Carl S. Apstein, MD; Ronglih Liao, PhD

Background—Myocardial infarction (MI) promotes deleterious remodeling of the myocardium, resulting in ventricular dilation and pump dysfunction. We examined whether supplementing infarcted myocardium with skeletal myoblasts would (1) result in viable myoblast implants, (2) attenuate deleterious remodeling, and (3) enhance in vivo and ex vivo contractile performance.

Methods and Results—Experimental MI was induced by 1-hour coronary ligation followed by reperfusion in adult male Lewis rats. One week after MI, 10^6 myoblasts were injected directly into the infarct region. Three groups of animals were studied at 3 and 6 weeks after cell therapy: noninfarcted control (control), MI plus sham injection (MI), and MI plus cell injection (MI+cell). In vivo cardiac function was assessed by maximum exercise capacity testing and ex vivo function was determined by pressure-volume curves obtained from isolated, red cell-perfused, balloon-in-left ventricle (LV) hearts. MI and MI+cell hearts had indistinguishable infarct sizes of $\approx 30\%$ of the LV. At 3 and 6 weeks after cell therapy, 92% (13 of 14) of MI+cell hearts showed evidence of myoblast graft survival. MI+cell hearts exhibited attenuation of global ventricular dilation and reduced septum-to-free wall diameter compared with MI hearts not receiving cell therapy. Furthermore, cell therapy improved both post-MI in vivo exercise capacity and ex vivo LV systolic pressures.

Conclusions—Implanted skeletal myoblasts form viable grafts in infarcted myocardium, resulting in enhanced post-MI exercise capacity and contractile function and attenuated ventricular dilation. These data illustrate that syngeneic myoblast implantation after MI improves both in vivo and ex vivo indexes of global ventricular dysfunction and deleterious remodeling and suggests that cellular implantation may be beneficial after MI. (*Circulation*. 2001;103:1920-1927.)

Key Words myocardial infarction ■ remodeling ■ exercise ■ myocardial contraction

Despite advances in the treatment of myocardial infarction (MI), congestive heart failure secondary to infarction continues to be a major complication. MI promotes acute and chronic transformation of both the necrotic infarct zone and the nonnecrotic, peri-infarct tissue, leading to global alterations that have collectively been termed “ventricular remodeling.”^{1–3} The cardiomyocytes lost during an MI cannot be regenerated, and the extent of the loss is inversely related to cardiac output, pressure-generating capacity, and, ultimately, survival.^{4,5} Cell therapy, or the supplementation of tissue with exogenous cells, has previously been used in the treatment of disease in which terminally differentiated cells are irreparably damaged.⁶ Recently, it has been suggested that cell therapy with skeletal myoblasts may be effective in the treatment of MI.^{7,8}

Myoblasts maintain the regenerative potential of skeletal muscle and, during periods of stress, proliferate and differentiate into myotubes, eventually forming new muscle fibers capable of contraction. Previous studies have shown that myoblasts implanted into myocardium undergo myotube formation, withdraw from the cell cycle, and remain viable.^{9,10} Furthermore, myoblasts implanted into cryoinfarcted myocardium have yielded similar results, with differentiation into slow-twitch skeletal myocytes expressing β -MHC and capable of contraction on stimulation.¹¹ Functional studies have also shown an improvement in regional contractility and compliance in cryoinfarcted myocardium after myoblast implantation.¹² We therefore hypothesized that supplementing infarcted myocardium with syngeneic skeletal myoblasts would result in the formation of viable muscle grafts capable

Received September 13, 2000; revision received November 1, 2000; accepted November 2, 2000.

From the Cardiac Muscle Research Laboratory (M.J., D.A.B., S.N., P.T., C.S.A., R.L.) and the Myocardial Biology Unit (D.B.S., W.S.C.), Boston University School of Medicine, Boston, Mass; and Diacrin, Inc (H.D., A.S.B.E., A.Z., K.W.), Charlestown, Mass.

*These authors contributed equally to this work.

Correspondence to Dr Ronglih Liao, Boston University School of Medicine, 650 Albany St, X-726, Boston, MA 02118. E-mail rliao@bu.edu

© 2001 American Heart Association, Inc.

Circulation is available at <http://www.circulationaha.org>

TABLE 1. Animal Characteristics

Time	Group	n	Body Weight, g	Heart Weight, g	Heart Weight/Body Weight	Lung Wet/Dry	Liver Wet/Dry
3 Wk after therapy	Control	9	358±7	1.16±0.06	3.23±0.15	4.88±0.05	3.31±0.01
	MI	6	347±5	1.44±0.03*	4.15±0.12*	4.83±0.08	3.28±0.07
	MI+cell	7	340±4	1.43±0.06*	4.11±0.08*	4.86±0.04	3.24±0.04
6 Wk after therapy	Control	9	391±7	1.18±0.06	3.01±0.13	4.94±0.04	3.26±0.01
	MI	7	398±8	1.54±0.05*	3.83±0.11*	4.97±0.02	3.25±0.01
	MI+cell	7	383±7	1.42±0.04*	3.70±0.17*	4.88±0.07	3.27±0.01

* $P<0.05$ vs control.

of attenuating deleterious post-MI remodeling and improving global cardiac performance. With the use of a rat coronary ligation model of MI,^{1,2,13} we demonstrate the physiological efficacy of myoblast implantation on both in vivo and ex vivo indexes of global cardiac remodeling and contractile failure.

Methods

Animal Model

Male inbred adult Lewis rats were obtained from Charles River Laboratories at 8 weeks of age, placed on a rat chow diet and water ad libitum, and housed under an alternating 12-hour light-dark cycle. Experimental MI was induced by coronary ligation of the main branch of the left marginal artery, as previously described.¹⁴ After 1 hour of coronary occlusion, the suture was removed, the myocardium reperfused, and the chest closed. Noninfarcted control animals

received an identical procedure with the exception of tying of the coronary suture. All animal handling and procedures strictly adhered to the regulations of Boston University Animal Care and the National Society for Medical Research.

Myoblast Generation and Cell Implantation

Myoblasts were isolated from skeletal hind leg muscle of neonatal Lewis rats. Neonatal tissue allowed for generation of a greater number of myoblast cells, with less fibroblast contamination, in a shorter time frame. We have previously isolated competent skeletal myoblasts from adult animals and humans with similar results.

Neonatal tissue was minced and digested (incubated at 37°C for 10 minutes) with a mixture of trypsin (0.5 mg/mL; GibcoBRL) and collagenase (0.5 mg/mL; GibcoBRL) to release satellite cells. Cell release was repeated 10 times for a given tissue isolation to maximize satellite cell recovery relative to contaminating fibroblasts. Cells from each isolation were seeded on poly-L-lysine/laminin (Sigma)-coated plates for expansion in myoblast growth basal

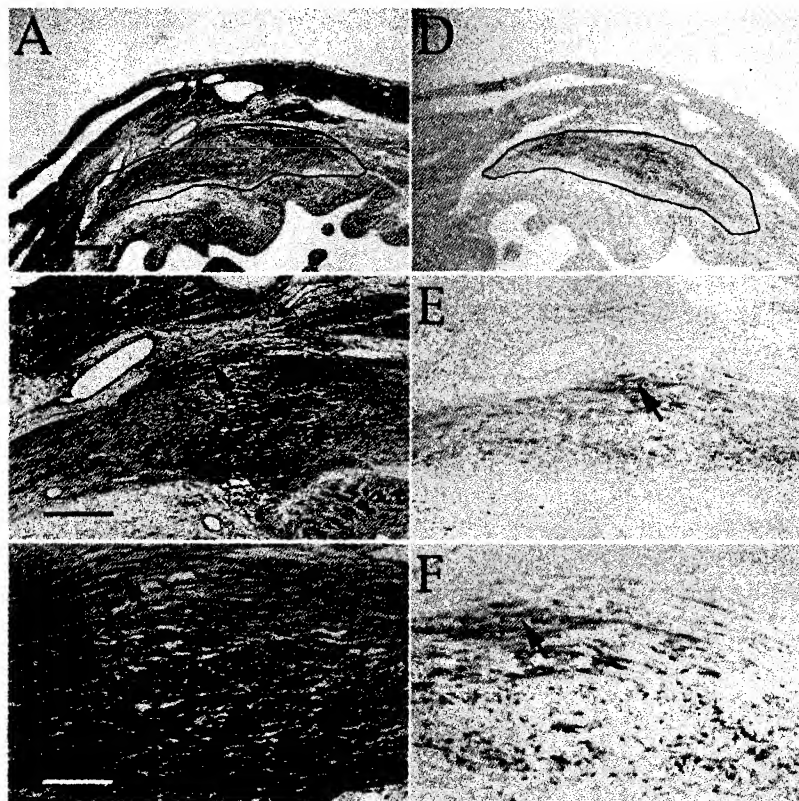


Figure 1. Myoblast survival in infarcted myocardium at 9 days after implantation. Infarcted LV free wall of rat is shown under increasing magnification with trichrome staining (A, B, and C) and immunohistochemical staining for myogenin (nuclear transcription factor unique to skeletal myoblasts) (D, E, and F). Under trichrome staining, replacement fibrosis appears blue and remaining viable myocardium red. Myogenin staining demonstrates presence of myoblasts within infarct region. Encircled area (A and D) identifies one area of graft survival within infarct region. Areas marked by arrows in B and E are shown under higher magnification in C and F, respectively. Bars represent distances of 1 mm in A and D; 200 μ m in B and E; and 100 μ m in C and F.

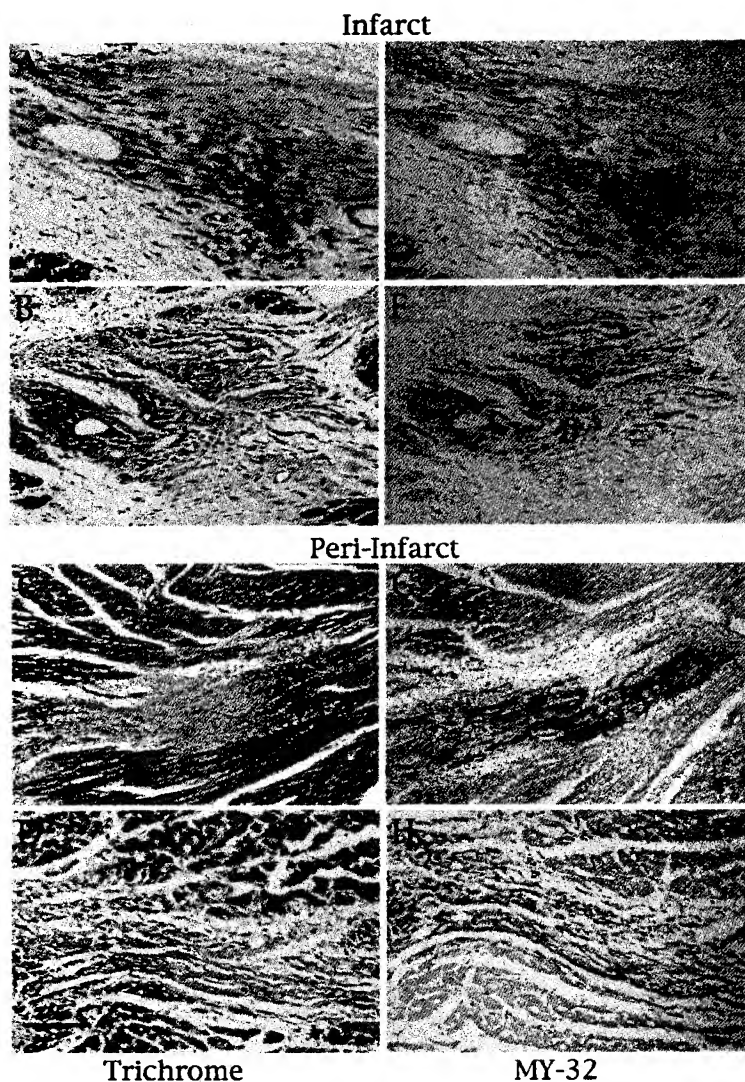


Figure 2. Myoblast survival in infarct and peri-infarct regions at 3 (A, C, E, and G) and 6 weeks (B, D, F, and H) after implantation. Corresponding tissue sections are shown with trichrome staining (A through D) and immunohistochemical staining for skeletal-specific myosin heavy chain (E through H). Viable cell grafts are demonstrated within infarct zone (upper 4 panels) and peri-infarct zone (lower 4 panels). Bar represents distance of 200 μ m in all panels.

medium (SkBM; Clonetics) containing 20% fetal bovine serum (Hyclone), recombinant human epidermal growth factor (rhEGF: 10 ng/mL), and dexamethasone (0.39 μ g/mL). Myoblast-enriched plates were identified after 48 hours of expansion and harvested with 0.05% trypsin-EDTA (GibcoBRL). For a given experiment, $\approx 10^7$ cells were harvested from 6 to 10 plates, seeded by satellite cells isolated from the limb muscle of 2 neonate equivalents. Similar results have been reported with adult skeletal muscle.^{11,12} Cells were washed and suspended in cold HBSS at 10^7 cells/mL and kept up to 4 hours on ice before injection. A total of 100 μ L (10^6 cells) was injected into each animal. Under these conditions, cells were determined to be $\approx 50\%$ myoblasts by flow cytometry with the monoclonal antibody H36 (anti-rat α -7 integrin).¹⁵ The remaining cells were fibroblast-like, as determined by cell morphology. The ability for myoblasts to fuse into multinucleated myotubes in vitro was also confirmed.

Seven days after MI, infarcted animals were randomized to receive cell or sham implantation. Rats underwent a second thoracotomy, and the left ventricle was visualized. Each rat received 6 to 10 injections (total of 10^6 cells/heart) of 10 to 16 μ L of myoblast suspension in HBSS directly into the infarct and peri-infarct regions, ≈ 1 to 2 mm apart, with a 30-gauge Hamilton needle. Infarcted animals not receiving cells underwent an identical injection proce-

dures with HBSS alone. Noninfarcted control animals were subjected to the same surgical procedures without injection.

Animal Groups

Three groups of animals were studied: control animals receiving neither infarction nor implantation (control), infarcted animals without cell therapy (MI), and infarcted animals receiving myoblast cell therapy (MI+cell). In vivo and ex vivo cardiac physiology and myoblast cell survival were studied at 3 and 6 weeks after cell therapy. Cell grafts were also examined at 9 days and 12 weeks after implantation in several animals to determine the time course of survival of implanted cells.

In Vivo Maximum Exercise Capacity

Maximum exercise capacity is often used as a measure of in vivo ventricular function and overall cardiac performance and recently has been demonstrated to be a valuable tool in the assessment of cardiac performance in smaller animal models.^{16,17} Maximum exercise capacity was assessed before implantation (1 week after MI) as well as at 3 and 6 weeks after implantation. Maximum exercise capacity was measured as the distance run on a modified rodent treadmill (Columbus Instruments) until exhaustion.¹⁸ Exhaustion

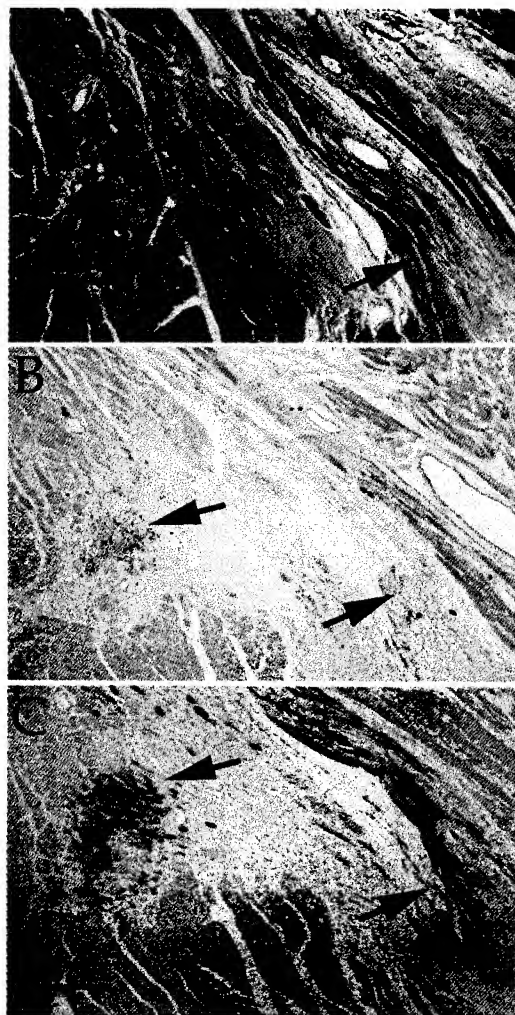


Figure 3. Myoblast survival in infarcted myocardium at 12 weeks after implantation. Infarcted LV free wall is shown with trichrome staining (A) and immunohistochemical staining for myogenin (B) or skeletal-specific myosin heavy chain (C). Myogenin and skeletal myosin heavy chain expression demonstrates presence of viable myoblasts and myotubes at 12 weeks after implantation. Bar represents distance of 200 μ m in A, B, and C.

was defined as the inability to run for 15 consecutive seconds despite minor electric shock. Initial treadmill speed was set at 15 m/min at a 15 degree grade and increased by 1-m/min increments every minute.

Ex Vivo Ventricular Function

To characterize myocardial remodeling and ex vivo cardiac function at 3 and 6 weeks after implantation, whole-heart Langendorff perfusion studies were performed in isolated isovolumically beating (balloon-in-left ventricle [LV]) hearts as previously described.^{19,20} Briefly, isolated hearts were retrogradely perfused with a perfusate consisting of bovine red blood cells suspended in modified Krebs-Henseleit buffer at a hematocrit of 40%. A fluid-filled cling-film balloon connected to a Statham P23Db pressure transducer (Statham Instruments) was placed into the left ventricle to monitor ventricular pressures. Coronary perfusion pressure was set to 80 mm Hg, and

active pressure-volume relations were then generated. From a balloon volume of zero, the balloon was filled in increments of 0.05 mL, and subsequent peak systolic and end-diastolic pressures were recorded. Systolic and diastolic pressure-volume relations were derived as previously described.^{19,20}

Tissue Histology and Morphometry

After pressure-volume experiments, hearts were arrested in diastole and fixed with 4% buffered paraformaldehyde at a final ventricular distending pressure of 5 mm Hg. Hearts were then weighed, paraffin-embedded, and sectioned (5 to 7 μ m thick) from each of 4 equally spread levels (atrium through apex).

Six-micron-thick sections were cut, mounted, and stained with trichrome. Myogenin immunohistochemistry was performed for identification of implanted skeletal myoblasts, whereas skeletal-specific myosin heavy chain immunohistochemistry was performed for identification of differentiated myotubes.⁹ For detection of myogenin, deparaffinized sections were blocked for endogenous peroxidase activity and subjected to antigen retrieval by boiling for 10 minutes in citrate buffer. Sections were blocked for endogenous biotin before adding primary polyclonal rabbit anti-rat myogenin antibody (Santa Cruz Biotechnology) followed by biotinylated goat anti-rabbit secondary antibody. For detection of myosin heavy chain, deparaffinized sections were incubated directly with alkaline phosphatase-conjugated MY-32 mAb (Sigma), specific for skeletal muscle myosin heavy chain, overnight at 4°C. Sections were developed with diaminobenzidine (DAB Substrate Kit; Vector) for myogenin or with BCIP-NBT (Zymed) for MY-32 mAb and counterstained with nuclear red or fast green.

In addition, trichrome sections were used for morphometric analysis. Stained sections were digitally imaged, and infarct size was determined as the mean percentage of epicardial and endocardial circumference occupied by scar tissue.²⁰ LV endocardial chamber diameter, septal wall thickness, and infarct wall thickness were derived from an average of 5 measurements taken throughout the respective regions.

Statistics

Data were analyzed by 1-factor ANOVA or paired *t* test where appropriate. Pressure-volume relations were analyzed by a 2-factor repeated-measures ANOVA and a least-significant-difference post hoc test. All data are presented as mean \pm SEM. A value of *P* < 0.05 was considered statistically significant.

Results

Animal Characteristics

Table 1 outlines the animal characteristics of control, MI, and MI+cell animals at both 3 and 6 weeks after therapy. All groups had a comparable increase in body weight over time. In addition, at all time points, hearts from MI and MI+cell groups displayed comparable degrees of LV hypertrophy of \approx 20% relative to control animals, as indicated by increased heart weights and heart-to-body weight ratios. Neither MI nor cell therapy altered lung or liver wet-to-dry ratios, suggesting the absence of pulmonary or hepatic congestion.

Animal Survival, Infarct Size, and Myoblast Implantation

Experimental MI resulted in \approx 15% acute mortality rate within 24 hours of operation, whereas the cell implantation procedure caused no additional animal deaths. Comparable infarct sizes of $31 \pm 1\%$ and $32 \pm 1\%$ of the LV were observed in MI and MI+cell hearts, respectively. Hearts receiving

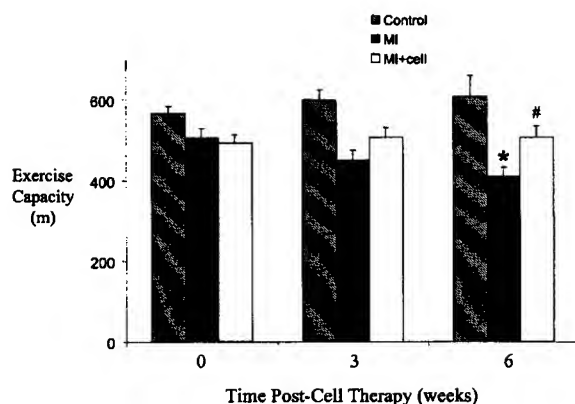


Figure 4. Maximum exercise capacity determined in noninfarcted control animals, MI rats, and MI+cell rats. Control animals maintained steady exercise performance over time. At all time points, MI and MI+cell animals had significant reduction in maximum exercise capacity relative to control animals ($P < 0.05$). MI rats had progressive decline in maximum exercise tolerance over time. Cell therapy prevented deterioration in post-MI exercise capacity. * $P < 0.05$ vs 0 weeks (pretherapy); # $P < 0.05$ vs MI.

infarction displayed areas of concentrated fibrosis, whereas noninfarcted control hearts appeared as continuous viable myocardium with homogenous thickness. Mortality rate was also similar in MI and MI+cell animals over the observation period, with no deaths at 3 weeks after implantation and 2 deaths in each group before assessment of cardiac function at 6 weeks after implantation.

Animals undergoing syngeneic cell therapy displayed no evidence for cell rejection as determined by excessive macrophage accumulation in tissue sections. Graft survival was identified at 9 days (Figure 1), 3 weeks (Figure 2, A, C, E, and G), 6 weeks (Figure 2, B, D, F, and H), and 12 weeks (Figure 3) after implantation, by immunohistochemical staining for myogenin (skeletal myoblasts) and for skeletal-specific myosin heavy chain (skeletal myotubes). Myogenin-positive staining was observed as early as 9 days (Figure 1, D, E, and F) and as late as 12 weeks after implantation (Figure 3B). Skeletal myosin heavy chain expression was not detected at 9 days after implantation (data not shown) and was first observed at 3 weeks after implantation (Figure 2, E and G). Continued skeletal myosin heavy chain staining was evident at 6 weeks (Figure 2, F and H) and 12 weeks (Figure 3C) after implantation.

Cell survival was confirmed in 6 of 7 animals at 3 weeks after therapy and in 7 of 7 animals at 6 weeks after therapy. At all examined time points, implanted cell grafts ranged in size from large patches of myoblasts and myotubes to uniformly dispersed single cells within both the infarct and adjacent peri-infarct regions. Examination of cell grafts at higher magnification indicated that after 3 weeks, implanted cells developed the elongated morphology characteristic of fused polynucleated myotubes. Implanted cells occasionally appeared to orient parallel to the endocardium and epicardium in similar alignment to cardiomyocytes. Furthermore, vascular structures were present within or adjacent to the

engrafted areas, suggesting that blood supply was available for implanted cells. In the nonnecrotic, peri-infarct region, implanted cells formed regions of myoblasts and myotubes surrounded by fibrosis (Figure 2, C and D).

Maximum Exercise Capacity

As seen in Figure 4, at baseline, before implantation, both MI and MI+cell animals exhibited comparable reductions in exercise capacity of $\approx 10\%$ relative to control animals, again suggesting similar degrees of myocardial damage before cell therapy. Control animals maintained a stable exercise capacity over the observation period. In contrast, MI animals exhibited a gradual decline in exercise performance with time, with a $>30\%$ reduction in exercise capacity relative to control animals at 6 weeks. Cell therapy, however, prevented the continued decline of post-MI exercise capacity, suggesting a protection against the progressive deterioration of in vivo cardiac function.

Ex Vivo Contractile Function

Cardiac contractile function was further investigated in isolated hearts through generation of systolic pressure-volume curves (Figure 5). Noninfarcted control hearts exhibited a typical rise in systolic pressure with increasing ventricular volume. Three weeks after implantation (4 weeks after MI), MI hearts displayed a rightward shift in the systolic pressure-volume curve (Figure 5A). Cell implantation prevented this shift in MI+cell hearts, resulting in greater systolic pressure generation at any given preload (ventricular volume). There was, however, no significant difference in the peak systolic pressure generated at maximum ventricular volume (at an end-diastolic pressure of 40 mm Hg) among groups. The beneficial effects of cell therapy were also seen at 6 weeks after therapy (Figure 5B), suggesting an improvement of ex vivo cardiac function with myoblast implantation.

Ventricular Dilation

In addition to pump dysfunction, ventricular remodeling characteristically results in progressive global cavity enlargement. Ventricular dilation was assessed with diastolic pressure-volume relations, established in isolated hearts through monitoring of distending pressures over a range of diastolic volumes (Figure 6). At all time points during the observation period, MI hearts exhibited substantially enlarged LVs relative to noninfarcted control hearts at any given distending pressure, demonstrated by a rightward repositioning of the pressure-volume curve. Cell therapy, however, caused a significant reduction in ventricular cavity dilation, placing hearts from the MI+cell group significantly leftward of the MI group at both 3 weeks (Figure 6A) and 6 weeks (Figure 6B) after implantation, thereby suggesting an attenuation of deleterious post-MI ventricular remodeling with cell implantation.

Ventricular Morphometry

Ventricular remodeling was further investigated through morphometric analysis of tissue sections (Table 2). At all time points, MI and MI+cell hearts exhibited enlarged chamber diameters compared with noninfarcted control hearts. Six

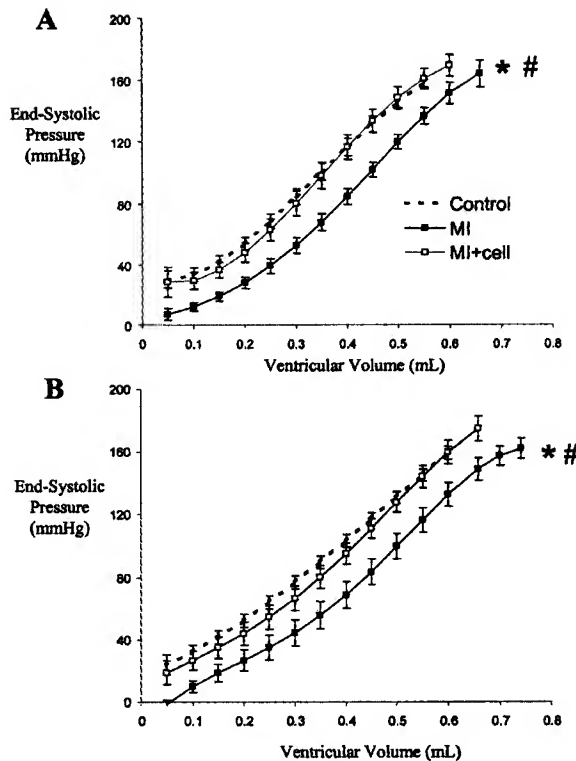


Figure 5. Systolic pressure-volume relations at 3 weeks after cell therapy (A) and 6 weeks after cell therapy (B) in noninfarcted control animals, MI rats, and MI+cell rats. Control hearts displayed characteristic increase in systolic pressure with increasing ventricular volume. MI hearts exhibited rightward shift in systolic pressure-volume curve. Cell therapy prevented shift in infarcted hearts, resulting in greater systolic pressures at given ventricular volume relative to MI hearts at both 3 and 6 weeks after cell therapy. * $P < 0.05$ vs control at any given ventricular volume; # $P < 0.05$ vs MI+cell at any given ventricular volume.

weeks after cell therapy, hearts from the MI+cell group had a reduced endocardial cavity diameter relative to MI hearts, suggesting an attenuation of ventricular dilation, similar as seen with diastolic pressure-volume curves in Figure 6B. In addition, MI hearts exhibited a decrease in infarct wall thickness at both 3 and 6 weeks after therapy, suggesting characteristic post-MI scar thinning and infarct expansion. MI

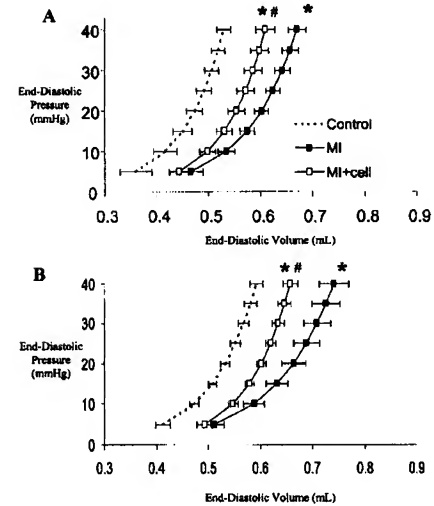


Figure 6. Diastolic pressure-volume relations at 3 weeks after cell therapy (A) and 6 weeks after cell therapy (B) in noninfarcted control animals, MI rats, and MI+cell rats. MI resulted in significant rightward shift of diastolic pressure-volume curve relative to noninfarcted control hearts. Cell therapy attenuated shift, suggesting reduction in ventricular global chamber dilation at both 3 and 6 weeks after cell therapy. * $P < 0.05$ vs control; # $P < 0.05$ vs MI.

hearts receiving cell therapy, however, had similar infarct wall thickness relative to both noninfarcted control and infarcted MI hearts. Septal wall thickness was comparable among all groups at both 3 and 6 weeks after therapy.

Discussion

Previous studies have suggested that implanted myoblasts form viable grafts with the potential to improve regional cardiac function in infarcted myocardium.^{9-12,21} Our experiments build on these initial studies and demonstrate the in vivo and ex vivo therapeutic benefits of myoblast implantation on global post-MI ventricular remodeling and cardiac function.

In this model of experimental MI, coronary occlusion release resulted in typical histological and physiological changes characteristic of deleterious post-MI ventricular remodeling,^{2,4} including an infarct region deficient in endogenous myocytes, infarct wall thinning, ventricular dilation,

TABLE 2. Ventricular Morphometry

Time	Group	LV Cavity Diameter, mm	Septum Thickness, mm	Infarct Wall Thickness, mm
3 Wk after therapy	Control	5.49±0.34	1.78±0.11	2.15±0.13
	MI	7.65±0.33†	1.68±0.19	1.44±0.24†
	MI+cell	6.77±0.13*	1.50±0.07	1.78±0.11
6 Wk after therapy	Control	5.93±0.24	1.75±0.07	2.01±0.06
	MI	8.11±0.43†	1.53±0.12	1.67±0.16*
	MI+cell	6.79±0.30*‡	1.63±0.07	1.77±0.19

* $P < 0.05$ vs control, † $P < 0.01$ vs control.

‡ $P < 0.05$ vs MI.

decreased ventricular function, and impaired exercise tolerance similar to previous reports.^{14,22–24} In addition, MI and MI+cell animals exhibited comparable infarct sizes and similar decreases in maximum exercise capacity before cell implantation, suggesting that differences in cardiac remodeling or function resulting from cell therapy were not due to disparities in initial ischemic injury. Cell implantation at 7 days after MI was selected on the basis of preliminary experiments indicating the greatest degree of cell survival relative to both longer and shorter post-MI time periods. Myoblast cell implantation resulted in focal areas of significant cell graft formation in >90% of animals tested.

LV cavity dilation and exercise intolerance are predictors of cardiovascular morbidity and are often used to gauge efficacy of experimental treatments and to guide therapy.^{25–28} Infarcted hearts receiving cell therapy had an attenuation of ventricular dilation assessed both in isolated hearts and LV cross sections. Cell implantation also improved ex vivo contractile function at 6 weeks after implantation and augmented in vivo maximum exercise capacity after MI. No apparent correlation, however, was observed between graft size and cardiac function.

Although global contractile function was increased after cellular implantation, it remains uncertain if implanted myoblasts are actively responsible for force generation during the cardiac cycle. Although several mechanisms may be responsible for the improved cardiac function, our data suggest that enhanced in vivo and ex vivo generated pressures are more likely to be a result of overall attenuation of deleterious ventricular remodeling within the infarcted and viable myocardium rather than an active force generation by myoblasts. In both animals and humans, myocardial pressure-generating capacity and corresponding exercise capacity decline gradually after MI as the infarcted and viable myocardium undergo progressive dilation and remodeling.^{2,28} Prevention of this dilation, even by physical restraint, results in increased cardiac performance.^{29,30} Therefore, implanted myoblasts may be responsible for augmented ventricular function through a mechanism involving attenuation of dilation of the viable myocardium and prevention of scar thinning, potentially through an increase in myocardial fibrosis. In addition, it is possible that growth factors, released by implanted cells, may exert a protective effect through stimulation of angiogenesis within the infarct and noninfarct regions.⁷

Cell therapy has been used effectively in the treatment of a variety of human disorders, from Parkinson's disease to diabetes, and holds promise in the therapy of many diseases in which nonregenerative cell death or abnormal cellular function plays a role. As with organ transplantation, the limitation of cell therapy revolves around both the availability of human cells and the possibility of immune rejection. It is for these reasons that skeletal myoblast implantation remains highly attractive as a potential medical treatment.⁸ Skeletal myoblasts are readily available and ensure immunological compatibility of myoblast cells cultured from a skeletal muscle biopsy of the recipient. In addition, myoblasts have been shown to have increased tolerance to ischemia⁷ and can survive in regions of reduced coronary perfusion, as is often present in patients

with coronary artery disease. These data illustrate the therapeutic benefits of syngeneic myoblast implantation after MI on both in vivo and ex vivo indexes of global ventricular dysfunction and deleterious remodeling and suggest that cell therapy may be beneficial after MI.

Acknowledgments

This work was funded by a research grant from Diacrin, Inc.

References

1. Pfeffer MA, Braunwald E. Ventricular remodeling after myocardial infarction: experimental observations and clinical implications. *Circulation*. 1990;81:1161–1172.
2. Ertl G, Gaudron P, Hu K. Ventricular remodeling after myocardial infarction: experimental and clinical studies. *Basic Res Cardiol*. 1993;88:125–137.
3. Anversa P, Li P, Zhang X, et al. Ischaemic myocardial injury and ventricular remodelling. *Cardiovasc Res*. 1993;27:145–157.
4. Pfeffer MA, Pfeffer JM, Fishbein MC, et al. Myocardial infarct size and ventricular function in rats. *Circ Res*. 1979;44:503–512.
5. Fletcher PJ, Pfeffer JM, Pfeffer MA, et al. Left ventricular diastolic pressure-volume relations in rats with healed myocardial infarction: effects on systolic function. *Circ Res*. 1981;49:618–626.
6. Deacon T, Schumacher J, Dinsmore J, et al. Histological evidence of fetal pig neural cell survival after transplantation into a patient with Parkinson's disease. *Nat Med*. 1997;3:350–353.
7. Leor J, Prentice H, Sartorelli V, et al. Gene transfer and cell transplant: an experimental approach to repair a "broken heart." *Cardiovasc Res*. 1997;35:431–441.
8. Reinlib L, Field L. Cell transplantation as future therapy for cardiovascular disease? A workshop of the National Heart, Lung, and Blood Institute. *Circulation*. 2000;101:E182–E187.
9. Koh GY, Klug MG, Soonpaa MH, et al. Differentiation and long-term survival of C2C12 myoblast grafts in heart. *J Clin Invest*. 1993;92:1548–1554.
10. Chiu RC, Zibaitis A, Kao RL. Cellular cardiomyoplasty: myocardial regeneration with satellite cell implantation. *Ann Thorac Surg*. 1995;60:12–18.
11. Murry CE, Wiseman RW, Schwartz SM, et al. Skeletal myoblast transplantation for repair of myocardial necrosis. *J Clin Invest*. 1996;98:2512–2523.
12. Taylor DA, Atkins BZ, Hungspreugs P, et al. Regenerating functional myocardium: improved performance after skeletal myoblast transplantation. *Nat Med*. 1998;4:929–933.
13. Fishbein MC, Maclean D, Maroko PR. Experimental myocardial infarction in the rat: qualitative and quantitative changes during pathologic evolution. *Am J Pathol*. 1978;90:57–70.
14. Youn TJ, Kim HS, Oh BH. Ventricular remodeling and transforming growth factor-beta 1 mRNA expression after nontransmural myocardial infarction in rats: effects of angiotensin converting enzyme inhibition and angiotensin II type 1 receptor blockade. *Basic Res Cardiol*. 1999;94:246–253.
15. Kaufman SJ, Foster RF, Haye KR, et al. Expression of a developmentally regulated antigen on the surface of skeletal and cardiac muscle cells. *J Cell Biol*. 1985;100:1977–1987.
16. Desai KH, Schauble E, Luo W, et al. Phospholamban deficiency does not compromise exercise capacity. *Am J Physiol*. 1999;276:H1172–H1177.
17. Desai KH, Sato R, Schauble E, et al. Cardiovascular indexes in the mouse at rest and with exercise: new tools to study models of cardiac disease. *Am J Physiol*. 1997;272:H1053–H1061.
18. Fewell JG, Osinska H, Klevitsky R, et al. A treadmill exercise regimen for identifying cardiovascular phenotypes in transgenic mice. *Am J Physiol*. 1997;273:H1595–H1605.
19. Eberli FR, Sam F, Ngoy S, et al. Left ventricular structural and functional remodeling in the mouse after myocardial infarction: assessment with the isovolumetrically contracting Langendorff heart. *J Mol Cell Cardiol*. 1998;30:1443–1447.
20. Jain M, Liao R, Ngoy S, et al. Angiotensin II receptor blockade attenuates the deleterious effects of exercise training on post-MI ventricular remodeling in rats. *Cardiovasc Res*. 2000;46:66–72.

21. Kao RL, Chin TK, Ganote CE, et al. Satellite cell transplantation to repair injured myocardium. *Cardiac and Vascular Regeneration*. 2000;1:31–42.
22. Oh BH, Ono S, Gilpin E, et al. Altered left ventricular remodeling with β -adrenergic blockade and exercise after coronary reperfusion in rats. *Circulation*. 1993;87:608–616.
23. Leor J, Patterson M, Quinones MJ, et al. Transplantation of fetal myocardial tissue into the infarcted myocardium of rat: a potential method for repair of infarcted myocardium? *Circulation*. 1996;94(suppl II):II-332–II-336.
24. Scorsin M, Hagege AA, Marotte F, et al. Does transplantation of cardiomyocytes improve function of infarcted myocardium? *Circulation*. 1997;96(suppl II):II-188–II-93.
25. Weber KT, Wilson JR, Janicki JS, et al. Exercise testing in the evaluation of the patient with chronic cardiac failure. *Am Rev Respir Dis*. 1984;129: S60–S62.
26. Riegger GA, Bouzo H, Petr P, et al. Improvement in exercise tolerance and symptoms of congestive heart failure during treatment with candesartan cilexetil: Symptom, Tolerability, Response to Exercise Trial of Candesartan Cilexetil in Heart Failure (STRETCH) Investigators. *Circulation*. 1999;100:2224–2230.
27. Kostuk WJ, Kazamias TM, Gander MP, et al. Left ventricular size after acute myocardial infarction: serial changes and their prognostic significance. *Circulation*. 1973;47:1174–1179.
28. Pfeffer MA, Pfeffer JM. Ventricular enlargement and reduced survival after myocardial infarction. *Circulation*. 1987;75(suppl IV):IV-93–IV-97.
29. Kelley ST, Malekan R, Gorman JH III, et al. Restraining infarct expansion preserves left ventricular geometry and function after acute anteroapical infarction. *Circulation*. 1999;99:135–142.
30. Schwarz ER, Speakman MT, Kloner RA. A new model of ventricular plication: a suturing technique to decrease left ventricular dimensions, improve contractility, and attenuate ventricular remodeling after myocardial infarction in the rat heart. *J Cardiovasc Pharmacol Ther*. 2000;5:41–49.

The 76th Annual Meeting

March 24-26, 2003

Fukuoka

Chairman: Yushi Ito

Abstract

Committee

Takashi Ishizaki	(Fac. Pharm., Kumamoto Univ.)
Hiroshi Ueda	(Fac. Pharm., Nagasaki Univ.)
Ryouzou Ohishi	(Kyushu Univ. Med. Hosp.)
Hirofumi Kai	(Fac. Pharm., Kumamoto Univ.)
Yasufumi Kataoka	(Fac. Pharm., Fukuoka Univ.)
Takeshi Katsuragi	(Fac. Med., Fukuoka Univ.)
Yuuzou Kato	(Fac. Den., Nagasaki Univ.)
Kenji Kitamura	(Fukuoka Den. Coll.)
Kayoko Kuroki	(Kyushu Den. Coll.)
Toshiyuki Sasaguri	(Grad. Sch. Med. Sci., Kyushu Univ.)
Kazuo Takahama	(Fac. Pharm., Kumamoto Univ.)
Masatoshi Tanaka	(Fac. Med., Kurume Univ.)
Kohtaro Taniyama	(Fac. Med., Nagasaki Univ.)
Ichiro Niki	(Ohita Med. Coll.)
Katsuhide Nishi	(Fac. Med., Kumamoto Univ.)
Masami Niwa	(Fac. Med., Nagasaki Univ.)
Chiaki Hara	(Daiichi Pharm. Coll.)
Masato Hirata	(Grad. Sch. Den. Sci., Kyushu Univ.)
Michihiro Fujiwara	(Fac. Pharm., Fukuoka Univ.)
Takeshi Miyata	(Fac. Pharm., Kumamoto Univ.)
Nobuyuki Yanagihara	(Sch. Med., Univ. Occup. Environ. Health)
Kenji Yamamoto	(Grad. Sch. Dent. Sci., Kyushu Univ.)
Shigenori Watanabe	(Grad. Sch. Pharm. Sci., Kyushu Univ.)

Secretariat

Ryuji Inoue

Department Pharmacology

**Graduate School of Medical Sciences
Kyushu University**

Fukuoka 812-8582

Phone: 092-642-6076

Fax: 092-642-6079

E-mail: inouery@pharmaco.med.kyushu-u.ac.jp

Journal of Pharmacological Sciences

Formerly *The Japanese Journal of Pharmacology*

<http://www.pharmacol.or.jp/>

Official Publication of The Japanese Pharmacological Society

Editor-in-Chief

Susumu Okabe (Kyoto, Japan)

Invited Editor

Yushi Ito (Fukuoka, Japan)

Press Editor

Yuji Ohizumi (Nagoya, Japan)

Associate Editors

Ezio Giacobini (Geneva, Switzerland)
(European Editor)

Hirofumi Kai (Kumamoto, Japan)

Kenji Kitamura (Fukuoka, Japan)

Mizuo Miyazaki (Takatsuki, Japan)

Yasushi Ohizumi (Sendai, Japan)

Tomio Okamura (Ohtsu, Japan)

Tsutomu Suzuki (Tokyo, Japan)

Katsutoshi Goto (Tsukuba, Japan)

Masahiro Kawamura (Tokyo, Japan)

Tony J.F. Lee (Springfield, IL, USA)
(North American Editor)

Masahiro Nishibori (Okayama, Japan)

Seitaro Ohkuma (Kurashiki, Japan)

Koki Shigenobu (Funabashi, Japan)

Hiroshi Ueda (Nagasaki, Japan)

Advisory Board

Y. Abe (Kagawa, Japan)

C.H. Cho (Hong Kong, China)

K. Fuji (Kyoto, Japan)

C. Hamada (Tokyo, Japan)

Y. Horio (Sapporo, Japan)

S. Kaneko (Kyoto, Japan)

H. Kogo (Hachioji, Japan)

K. Löffelholz (Mainz, Germany)

K. Miyata (Tsukuba, Japan)

K. Ohya (Tokyo, Japan)

M. Sakanashi (Okinawa, Japan)

T. Tamaki (Tokushima, Japan)

H. Tsuru (Tokyo, Japan)

K. Umemura (Hamamatsu, Japan)

K. Yamamoto (Fukuoka, Japan)

S. Yano (Chiba, Japan)

Y. Ashida (Osaka, Japan)

P. Dominiak (Lübeck, Germany)

K. Fukunaga (Sendai, Japan)

E. Hamel (Montreal, Canada)

R. Inoue (Fukuoka, Japan)

H. Kawasaki (Okayama, Japan)

S. Kohno (Kyoto, Japan)

M. Misawa (Tokyo, Japan)

H. Nakaya (Chiba, Japan)

J. Oka (Noda, Japan)

T. Tadano (Sendai, Japan)

J. Tamargo (Madrid, Spain)

M.K. Uchida (Kiyose, Japan)

T. Urushidani (Tokyo, Japan)

A. Yamatodani (Suita, Japan)

T. Yoshida (Tokyo, Japan)

J.E. Brayden (Burlington, VT, USA)

A. Fisher (Ness Ziona, Israel)

M.C.E. Gwee (Singapore)

F. Hata (Sakai, Japan)

K. Ishii (Tokyo, Japan)

M.-S. Kim (Seoul, Korea)

M.D. Linnik (San Diego, CA, USA)

K. Miyamoto (Kanazawa, Japan)

Y. Ohno (Tokyo, Japan)

G. Pepeu (Florence, Italy)

K. Takeuchi (Kyoto, Japan)

L.F. Tseng (Milwaukee, WI, USA)

M. Ukai (Nagoya, Japan)

K. Yamada (Kanazawa, Japan)

N. Yamazaki (Osaka, Japan)

Editorial Assistant

Y. Takezaki

The Japanese Pharmacological Society

Board of Directors: K. Hashimoto (President), A. Akaike, A. Baba, M. Endoh, H. Endou, K. Honda, Y. Ito (Chairman of the Annual Meeting), H. Karaki, Y. Kudo, N. Matsuki, N. Miki, M. Minami, T. Nabeshima, T. Nagao, S. Narumiya, S. Okabe, M. Satoh, K. Taniyama, Z. Terashita;

Auditors: K. Momose, T. Nakashima

The cover illustration was designed by Ms. Kyoko Terada, who modeled her images on a drawing found on an ancient Greek cup (ca. 600 BC). The figure illustrates workers weighing the precious drug Sylfium, a plant cathartic, under the supervision of a King, in preparation for export to foreign countries. In that time, due to its pharmacological efficacy, Sylfium was worth its weight in gold.

1P252

Cardiac troponin T (cTnT) is a superior marker to creatine phosphokinase (CPK) for myocardial dysfunction in rats with myocardial infarction. Yukiko Morimoto, Chikaomi Yamada, Hiromitsu Takagi, Takehiko Iwaki, Akira Mizuno and Mayumi Furuya. Suntory Biomed. Res. Ltd., Osaka 618-8503, Japan.

Both cTnT and CPK are clinically used as biomarkers of myocardial injury. In the present study, we prepared a rat model of myocardial infarction by 30min coronary ligation and reperfusion, and compared the plasma cTnT and CPK concentrations after ischemia-reperfusion with the infarct size. We also investigated the effect of 3-aminobenzamide (3-AB), a poly(ADP-ribose) polymerase (PARP) inhibitor, on the plasma cTnT level and myocardial infarct size. Plasma cTnT concentrations were markedly increased after myocardial ischemia-reperfusion, and peaked 2 hours after reperfusion, which were then gradually decreased, but still higher than those of sham-operated rats even 24 hours after reperfusion. At any time point, plasma cTnT concentrations positively correlated with the infarct size. Plasma CPK levels also tended to increase 2 hours after reperfusion, but had no correlations with the infarct size. Intravenous administration of 3-AB (10 mg/kg + 10 mg/kg/hr) at 10 min before reperfusion significantly reduced both plasma cTnT concentrations and the infarct size 2 hours after reperfusion. These results suggest that plasma cTnT concentrations could be a superior biomarker to plasma CPK to detect myocardial dysfunction, and that PARP inhibitor has a therapeutic value for myocardial protection.

1P254

Effect of shear stress on methoxamine-induced vasoconstriction in rat mesenteric arterial bed. Atsushi Sato, Hiroshi Suenaga and Katsuo Kamata. Dept. Physiol. Morphol., Inst. Medicinal Chem., Hoshi Univ., Shinagawa-ku, Tokyo 142-8501, Japan.

The aim of present study was to examine the effects of shear stress on the contractile responses of rat mesenteric arterial bed to methoxamine (Met). The arterial bed was perfused with modified Krebs-Henseleit solution (flow rate of 5 mL/min) in the absence or presence of 4% bovine serum albumin (BSA) to enhance viscosity. Met increased the perfusion pressure in a dose dependent manner and these constrictions were not altered by L-arginine treatment. The Met-induced constriction was not also inhibited by BSA contained solution. However, treatment with both L-arginine and BSA markedly inhibited the Met-induced response. Treatment of the mesentery bed with both N ω -nitro-L-arginine methyl ester (L-NAME; 0.1mM) and N ω -nitro-L-arginine (L-NA; 0.1mM) strongly potentiated Met-induced constriction. In the presence of these inhibitors, the shear stress-induced inhibition was not observed. Typhostin-A23, a tyrosine kinase inhibitor (0.3mM), did not inhibit Met-induced response, but it selectively abolished the inhibitory effect by shear stress. The release of NO $_2^-$ plus NO $_3^-$ into the perfusate was significantly increased by the treatment with both L-arginine and BSA. These results suggest that shear stress attenuates Met-induced vasoconstriction by influx of extracellular L-arginine and that tyrosine kinase activity may be involved in these actions.

1P253

Effects of SEA0400, a novel inhibitor of Sodium-Calcium exchanger, on electrical and mechanical activities of myocardia. Tokiko Aikawa¹, Wataru Hirayama², Taro Kawanura², Hiroyuki Masuda², Kazuhide Nishimaru², Haruko Masumiya², Hikaru Tanaka², Toru Kawanishi² and Koki Shigenobu¹

¹Dept. Pharmacol., Toho Univ. Sch. Pharm. Sci., Funabashi 274-8510, ²Div. Biol. Chem.Biol., Natl. Inst. Health. Sci., Tokyo 158-8501, Japan.

SEA0400 is a novel inhibitor of the Na⁺-Ca²⁺ exchanger (NCX), developed by prof. Akemichi Baba et al. and Taisho Pharmaceutical Co. Ltd. In voltage clamped guinea-pig ventricular myocytes, SEA0400 concentration-dependently inhibited the NCX current (Tanaka et al., Brit. J. Pharmacol. 135: 1096-1100, 2002) but had no significant effect on other membrane currents (I_{Na}, I_{CaL}, I_{K1}, I_K).

SEA0400 had no effect on beating rate of the guinea pig right atria and SA node action potential configuration of rabbit. SEA0400 increased contractile force in the guinea pig, rat and mouse ventricle; this was accompanied by increased Ca²⁺ transient amplitude. SEA0400 concentration-dependently suppressed ouabain induced positive inotropy in the guinea pig.

SEA0400 had no significant effect on action potential parameters such as RP (resting potential), OS (overshoot), AMP (amplitude), APD (action potential duration) and V_{max} in the guinea pig. In the rat and mouse ventricle, SEA0400 shortened the late plateau, which is considered to reflect Ca²⁺ extrusion by NCX.

These results indicate that SEA0400 is a powerful tool for further studies on the role of NCX in the heart.

1P255

Serum lipocalin-type prostaglandin D synthase as a sensitive marker for atherosclerosis. Nanae Taniguchi¹, Yoji Kato², Yutaka Eguchi³, Kosuke Aritake⁴, Hiroshi Oda⁴, Naomi Eguchi⁴ and Yoshihiro Urade¹. ¹Dept. Mol. Behav. Biol., Osaka Biosci. Inst., Suita 565-0874, ²Cardiovas. Div., ISHINKAI YAO Gen. Hosp., Yao 581-0036, ³Intensive Care Unit, Shiga Univ. Med. Sci., Otsu, Shiga 520-2192, ⁴Cen. Res. Inst. Maruha Corp., Tsukuba 300-4295, Japan.

In the cardiovascular system, prostaglandin (PG) D₂ shows several actions such as inhibiting platelet aggregation and induction of vasodilation. We recently reported that lipocalin-type PGD synthase (L-PGDS) was localized in the human synthetic phenotype of smooth muscle cells, and was secreted into the coronary circulation (Eguchi Y et al., PNAS 94, 14689-94, 1997). In this study, we measured the serum concentration of L-PGDS using the blood samples taken from the ascending aorta and great cardiac vein in patients with chest symptoms who were investigated by coronary angiography. The venous level of L-PGDS was higher than the aortic level, and the veno-aortic difference was increased depending on the severity of disease in the coronary, but not leg, circulation. However, no veno-aortic difference was found in lipoprotein (a) and C-reactive protein levels. In autopsy specimens, the L-PGDS immunoreactivity was decreased in endothelial cells and inversely increased in smooth muscle cells and extracellular matrix of the coronary arteries with early atherosclerosis and of atheromatous vein graft. Therefore, serum L-PGDS is useful as a marker for coronary atherosclerosis.